nature aging

ARTICLES

https://doi.org/10.1038/s43587-022-00187-y

Check for updates

Age-associated impairment of T cell immunity is linked to sex-dimorphic elevation of N-glycan branching

Haik Mkhikian[1,8], Ken L. Hayama[2,8], Khachik Khachikyan[3], Carey Li[3], Raymond W. Zhou[3], Judy Pawling[4], Suzi Klaus[2], Phuong Q. N. Tran[3], Kim M. Ly[3], Andrew D. Gong[3], Hayk Saryan[3], Jasper L. Hai[3], David Grigoryan[3], Philip L. Lee[3], Barbara L. Newton[3], Manuela Raffatellu[2,5,6], James W. Dennis[4,7] and Michael Demetriou[2,3] ✉

Impaired T cell immunity with aging increases mortality from infectious disease. The branching of asparagine-linked glycans is a critical negative regulator of T cell immunity. Here we show that branching increases with age in females more than in males, in naive T cells (T_N) more than in memory T cells, and in $CD4^+$ more than in $CD8^+$ T cells. Female sex hormones and thymic output of T_N cells decrease with age; however, neither thymectomy nor ovariectomy altered branching. Interleukin-7 (IL-7) signaling was increased in old female more than male mouse T_N cells, and triggered increased branching. N-acetylglucosamine, a rate-limiting metabolite for branching, increased with age in humans and synergized with IL-7 to raise branching. Reversing elevated branching rejuvenated T cell function and reduced severity of *Salmonella* infection in old female mice. These data suggest sex-dimorphic antagonistic pleiotropy, where IL-7 initially benefits immunity through T_N maintenance but inhibits T_N function by raising branching synergistically with age-dependent increases in N-acetylglucosamine.

Aging-associated immune dysfunction, referred to as immunosenescence, contributes to increased morbidity and mortality from both infectious and neoplastic diseases in older adults (adults ≥65 years old)[1,2]. For example, around 89% of annual deaths from influenza in the USA are in people at least 65 years old, despite this age group representing only around 15% of the US population[3]. The vulnerability of older adults to viral infections has been tragically highlighted by the recent emergence of severe acute respiratory syndrome coronavirus 2 (SARS-CoV-2)[4]. Increased morbidity and mortality in older adults also occurs with common bacterial infections such as those caused by the enteric pathogen *Salmonella*[5]. Furthermore, efficacy of immunizations declines with age[6,7], further increasing risk of infection in older adults. The rapidly aging population in the developed world exacerbates this issue and heightens the need for interventions that effectively target immunosenescence.

A number of age-associated changes in T cell numbers and functionality have been identified. The frequencies of T_N versus central and/or effector memory T cells change substantially with age in both mice and humans, as the accumulation of antigenic experience promotes conversion of naive cells to memory cells. T_N cell numbers are maintained by production of new T_N cells in the thymus and by IL-7 dependent homeostatic proliferation in the periphery[8]. In mice, although the thymus involutes with age, thymic production remains a main contributor of T_N cell production throughout much of adult life. In humans, by contrast, thymic production decreases dramatically early in life and T_N cell numbers are maintained primarily through peripheral IL-7-dependent proliferation[9]. Despite these changes, the size of the $CD4^+$ T_N cell pool is largely maintained throughout life and the T cell receptor (TCR) repertoire decreases only mildly[10]. T cell function is also altered with age, with $CD4^+$ T_N cells exhibiting diminished signaling and activation in response to TCR stimulation[11]. However, despite the identification of multiple contributing deficits in T cell dysfunction, the underlying molecular mechanisms remain incompletely understood.

Asparagine (N)-linked glycans play a critical role in controlling T and B cell immunity in mice and humans[12–22]. The endoplasmic reticulum (ER)/Golgi secretory pathway in animal cells modifies nearly all cell-surface and secreted proteins via addition of complex carbohydrates. As these glycoproteins transit through the secretory pathway, their N-glycans are further modified by a set of resident glycosylation enzymes. N-acetylglucosaminyltransferases I, II, III, IV, and V (encoded by *Mgat1*, *Mgat2*, *Mgat3*, *Mgat4a/b* and *Mgat5*) initiate N-acetylglucosamine (GlcNAc) branches that are variably extended/modified with galactose, sialic acid, fucose and/or sulfate (Extended Data Fig. 1a). This remodeling regulates ligand production for multivalent animal lectins (for example, galectins, siglecs and C-type lectins). Our work has revealed that galectins bind TCR and other glycoproteins at the cell surface, forming a molecular lattice that impacts clustering, signaling and endocytosis of surface receptors and transporters to affect cell growth, differentiation and disease states in mice and humans[12–21,23–26]. In T cells, N-glycan

[1]Department of Pathology and Laboratory Medicine, University of California, Irvine, Irvine, CA, USA. [2]Department of Microbiology and Molecular Genetics, University of California, Irvine, Irvine, CA, USA. [3]Department of Neurology, University of California, Irvine, Irvine, CA, USA. [4]Lunenfeld-Tanenbaum Research Institute, Mount Sinai Hospital, Toronto, Ontario, Canada. [5]Division of Host-Microbe Systems and Therapeutics, Department of Pediatrics, University of California, San Diego, La Jolla, CA, USA. [6]Center for Mucosal Immunology, Allergy, and Vaccines, Chiba University-UC San Diego, La Jolla, CA, USA. [7]Department of Molecular Genetics, University of Toronto, Toronto, Ontario, Canada. [8]These authors contributed equally: Haik Mkhikian, Ken L. Hayama. ✉e-mail: mdemetri@uci.edu

branching and the galectin lattice negatively regulate TCR clustering/signaling, promote surface retention of cytotoxic T-lymphocyte antigen 4 (CTLA-4), inhibit inflammatory T_H1 and T_H17 while promoting anti-inflammatory T_H2 and induced T regulatory cell (iTreg) differentiation and suppress development of autoimmunity in mice and humans[12–18,20,27,28].

The degree of N-glycan branching is among the main determinants of galectin lattice strength. Branching is regulated, in turn, by a complex network of genetic, metabolic and environmental factors that converge on the N-glycan branching pathway. These include multiple disease-associated polymorphisms, dietary intake of glycan building blocks, and metabolic production of uridine diphosphate GlcNAc (UDP-GlcNAc)—the common nucleotide sugar substrate of the branching enzymes. UDP-GlcNAc is produced either by de novo synthesis from glucose via the hexosamine pathway or by salvage of GlcNAc. In vitro and in vivo supplementation with GlcNAc enhances N-glycan branching in T cells and suppresses autoimmunity[16,17,29].

Given the importance of N-glycans in regulating T cell function, we investigated whether N-glycan branching is altered with age. Indeed, we discovered that aging in female over male mice and humans is associated with increases in branched N-glycans in T_N cells, and that reversing this phenotype rejuvenates T cell responses. We further uncover that this sex-dimorphic trait arises from excessive IL-7 signaling in mice and synergy with age-dependent increases in serum GlcNAc in humans, identifying novel therapeutic targets for immunosenescence.

Results

N-glycan branching increases with age in female more than in male mouse T cells. To explore whether N-glycan branching increases with age, we compared L-PHA binding (*Phaseolus vulgaris*, leukoagglutinin) in splenic mouse T cells from old (74–113 weeks) and young (7–32 weeks) adult mice. L-PHA binds to β1,6GlcNAc-branched N-glycans (Extended Data Fig. 1a) and serves as a highly sensitive and quantitative marker of branching[14,30]. Flow cytometry revealed significant increases in branching in female splenic $CD4^+$ T cells, with differences being T_N > central memory (T_{CM}) > effector memory (T_{EM}) cells (Fig. 1a–c and Extended Data Fig. 1b,c). Consistent with elevated branching, high-mannose structures as measured by conconavalin A (ConA) binding were reduced in old female $CD4^+$ T_N cells (Extended Data Fig. 1a,d). Female $CD4^+$ T_N cells from peripheral lymph nodes were similarly elevated (Extended Data Fig. 1e). As a change in branching of only around 20% is sufficient to alter T cell function and inflammatory disease risk[29,30], the observed increases are biologically significant. The L-PHA binding of both young and old female T_N cells follows a similar Gaussian distribution, demonstrating that branching is elevated in the entire population and not due to unaccounted for heterogeneity in the $CD4^+$ T_N cell gate (Fig. 1b). In contrast, L-PHA histograms of the memory populations demonstrated broader multimodal peaks that shifted toward higher average mean fluorescence intensities (MFIs) but remain overlapping when comparing young and old. This suggests that, unlike T_N cells, the smaller increases in L-PHA binding in the memory populations may be due, in part or completely, to shifts in unaccounted for subset frequencies.

Strikingly, although L-PHA binding in old male T_N and memory $CD4^+$ T cells was also elevated relative to young cells (Fig. 1d and Extended Data Fig. 1f), the effect was less consistent and of a markedly smaller magnitude than for old female $CD4^+$ T cells (for example, a mean increase of 17.1% for male versus 70.2% for female $CD4^+$ T_N cells) (Fig. 1c,d and Extended Data Fig. 1g). T_N but not memory female $CD8^+$ T cells also showed elevated L-PHA binding relative to young cells (Fig. 1e), while male $CD8^+$ T cells again showed smaller age-dependent differences (Fig. 1f). $CD19^+$ B cells in both males and females lacked notable differences in L-PHA binding with age (Extended Data Fig. 1h). T_N output from the thymus decreases significantly in old mice. Although N-glycan branching regulates T cell production from the thymus[27], single and double positive thymocytes exhibited no age-dependent differences in L-PHA binding (Extended Data Fig. 1i). This indicates that the increase in N-glycan branching in old T_N cells arises in the periphery rather than from alterations in thymocyte development in old mice. Together, these data show that N-glycan branching increases more with age in female than male mouse T cells, with the greatest difference being in the $CD4^+$ T_N subset.

IL-7 signaling increases with age to raise N-glycan branching. To identify potential mechanisms driving elevated branching, we first sought to determine whether increased branching in old female T_N cells arises from cell-intrinsic and/or cell-extrinsic factors. To assess this, we normalized the environment of $CD4^+$ T cells from young and old female mice by culturing them in media for 3 days in vitro. Indeed, equalizing external factors significantly reduced the difference in N-glycan branching between young and old female $CD4^+$ T_N cells, albeit aged T cells still retained higher branching compared with young T cells (Fig. 2a). Similarly, adoptively transferring congenically marked old female $CD4^+$ T_N cells into young recipient female mice for 2 weeks also significantly reduced the difference in N-glycan branching between young and old $CD4^+$ T_N cells (Fig. 2b and Extended Data Fig. 2a). Thus, cell-extrinsic factors in old female mice primarily drive increases in N-glycan branching.

To further explore the mechanism, we sought to leverage the striking sex difference of the age-associated elevation in branching. We reasoned that age-associated gene-expression changes enriched in female compared with male T cells, and T_N compared with T_{EM} cells were likely involved. We thus performed RNA-sequencing (RNA-seq) analysis on fluorescence-activated cell sorting (FACS) sorted, highly purified young and old $CD4^+$ T_N and T_{EM} cells from female and male mice with representative changes in branching (Extended Data Fig. 2b,c). Principal component analysis revealed that $CD4^+$ T_N clustered tightly together regardless of age and sex (Extended Data Fig. 2c). Moreover, the T_N population was widely separated from the T_{EM} cell populations, indicating that the purified $CD4^+$ T_N cells are not appreciably contaminated by memory cells. Comparing young and old $CD4^+$ T_N cells, 158 and 192 differentially expressed genes (DEGs) were identified in females and males, respectively. Remarkably, only 44 of these overlapped between the sexes (Extended Data Fig. 2d and Supplementary Tables 1–3). There were no significant differences in gene expression of N-glycan branching enzymes or other relevant glycosylation genes (Supplementary Table 4), which we confirmed by quantitative PCR (qPCR) for critical Golgi branching enzymes (Extended Data Fig. 2e).

Among the 114 DEGs in female but not male $CD4^+$ T_N cells, 4 were in the IL-7 signaling pathway (Table 1)—a pathway previously implicated in regulating N-glycan branching[17]. This included reduced expression of IL-7 receptor alpha chain (*Il7r*) and increased expression of Suppressor of cytokine signaling 1 (*Socs1*), *Socs3* and Janus kinase 3 (*Jak3*). Other IL-7 signaling pathway genes were unchanged (Table 1). Flow cytometry confirmed that IL7Rα protein was reduced more in aged female than in male $CD4^+$ T_N cells (Fig. 2c and Extended Data Fig. 2f) and correlated strongly with the magnitude of branching elevation (Extended Data Fig. 2g). In contrast, IL7Rα protein expression was unchanged in old male and female $CD4^+$ T_{EM} cells (Extended Data Fig. 2h,i). IL-7 signaling is known to downregulate IL7Rα levels, suggesting that the decrease observed may be secondary to excessive IL-7 signaling in old female T_N cells[8,31]. Indeed, IL7Rα levels and phosphorylation of the downstream signaling molecule STAT5 (pSTAT5) are proxy measures of IL-7 signaling[32]. Consistent with this hypothesis and the observed IL7Rα expression levels, old female $CD4^+$ T_N cells but not T_{EM} cells

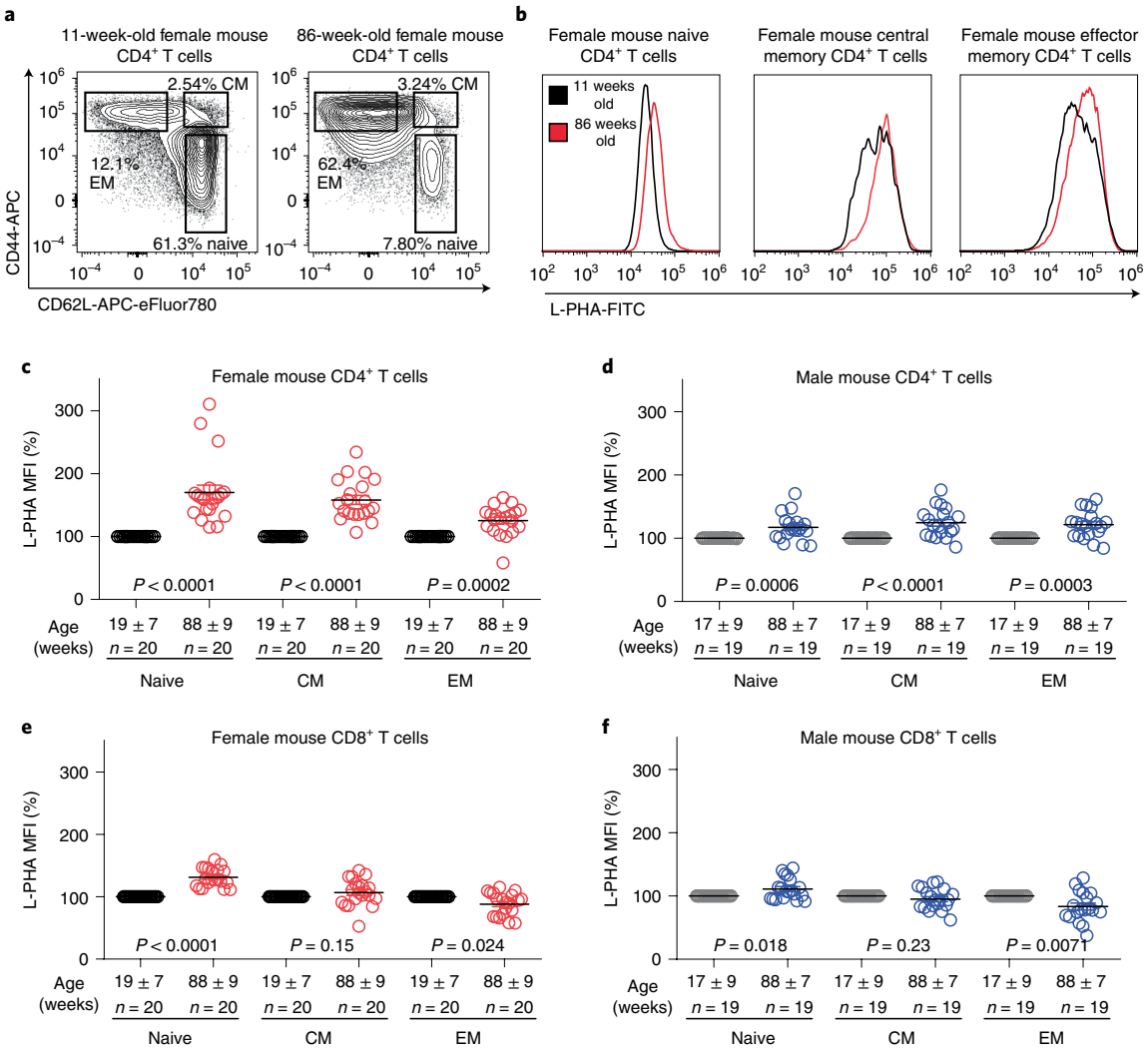

Fig. 1 | Mouse T cells show a sex-dimorphic increase in N-glycan branching with age. a, Splenic T cells from representative young and old female mice were stained for naive and memory markers, demonstrating naive(CD62L$^+$CD44$^-$), central memory (CM) (CD62L$^+$CD44$^+$) and effector memory (EM) (CD62L$^-$CD44$^-$) subsets. **b**, L-PHA staining histograms of young and old female CD4$^+$ naïve, CM and EM T cell subsets. **c**–**f**, Splenic T cells from 20 young (range 7–32 weeks) and 20 old (range 74–113 weeks) female, as well as 19 young (range 7–31 weeks) and 19 old (range 80–100 weeks) male mice were analyzed in pairs by flow cytometry for L-PHA binding on naïve, CM, or EM subsets. Analyses of female CD4$^+$ (**c**), male CD4$^+$ (**d**), female CD8$^+$ (**e**) and male CD8$^+$ (**f**) T cells are shown. Each symbol represents a single mouse. Each old mouse was normalized to its young control. Age of mice in weeks with s.d. is shown. *P*-values by two-tailed Wilcoxen test. Error bars indicate mean ± s.e.m.

showed increased basal pSTAT5 (Fig. 2d). Note that IL-7 has a short serum half-life in mice (around 2 h) and was not detectable by enzyme-linked immunosorbent assay (ELISA) in the serum of old female mice.

To examine directly whether increased IL-7 signaling enhances N-glycan branching, we cultured old and young resting CD4$^+$ T cells with recombinant IL-7. Indeed, IL-7 significantly increased N-glycan branching in both old and young, male and female CD4$^+$ T_N cells (Fig. 2e,f), with no differences noted between the sexes. To confirm that IL-7 signaling also increases N-glycan branching in CD4$^+$ T_N cells in vivo, we administered IL-7 as a complex with the anti-IL-7 monoclonal antibody M25 into young mice. As a preformed complex, IL-7/M25 improves IL-7 halflife and markedly increases biological activity in vivo[33]. The IL-7/M25 complex at two different doses significantly increased N-glycan branching levels in CD4$^+$ T_N cells of young mice in vivo (Fig. 2g). To confirm that excessive IL-7 signaling was increasing N-glycan branching in CD4$^+$ T_N cells of old female mice, we injected high doses of the anti-IL-7 M25 antibody, which blocks endogenous IL-7 signaling at these doses[34]. Indeed, 2 weeks of anti-IL-7 antibody (M25) treatment reduced N-glycan branching levels in old female CD4$^+$ T_N cells down to that of young cells in both blood and spleen (Fig. 2h,i). This treatment also seemed to partially reverse the reduction in IL7Rα protein expression present in old female CD4$^+$ T_N cells (Extended Data Fig. 2j). As 2 weeks of inhibiting IL-7 may be too short to fully reverse the downregulation of IL7Rα, we repeated the anti-IL-7 antibody (M25) treatment for 4 weeks. In addition to lowering N-glycan branching (Extended Data Fig. 2k,l), the longer treatment reversed the reduction in IL7Rα protein expression as well as the elevation in basal pSTAT5 levels in old female CD4$^+$ T_N cells (Fig. 2j,k). These reversals confirm that excessive IL-7 signaling in vivo is responsible for reduced IL7Rα and elevated basal pSTAT5 in old female mice. More broadly, the combined data indicate that a sex-dimorphic elevation of IL-7 signaling raises N-glycan branching in old female more than male CD4$^+$ T_N cells.

IL-7 is critical for homeostatic maintenance of T cells and may be increased coincident with thymic involution as T cells rely more on homeostatic proliferation. Alternatively, with reduced thymic

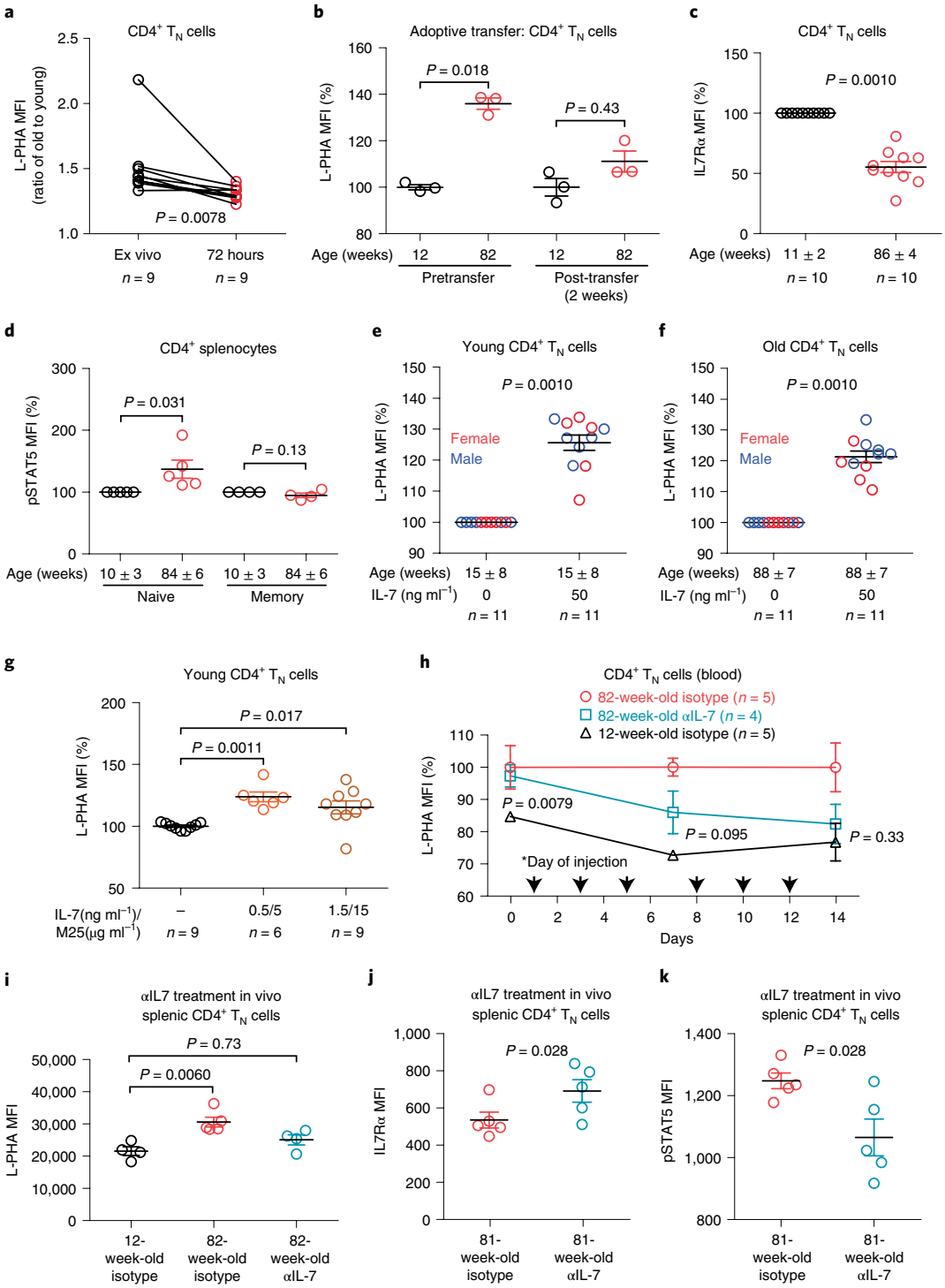

Fig. 2 | Elevated IL-7 signaling increases N-glycan branching in old female CD4$^+$ T$_N$ cells. a, L-PHA flow cytometry of splenocytes gated on CD4$^+$ T$_N$ cells from young (12 ± 4 weeks old) and old (86 ± 3 weeks old) female mice immediately ex vivo and after 72 h of rest in culture. Shown is L-PHA MFI ratio in old over young. **b**, Old and young female CD45.2$^+$ CD4$^+$ T$_N$ cells were adoptively transferred into young female CD45.1$^+$ recipient mice and analyzed by flow cytometry for L-PHA binding pre- and 2 weeks post-transfer, gating on CD4$^+$ T$_N$ cells. **c**,**d**, Flow cytometric analysis of IL7Rα (**c**) and pSTAT5 (**d**) in ex vivo naive (**c**,**d**) and total memory (CD44$^+$) (**d**) CD4$^+$ T cells from young and old female mice. **e**,**f**, Flow cytometric analysis of L-PHA binding on CD4$^+$ T$_N$ cells from young (**e**) and old (**f**) female (red) and male (blue) mice treated with or without rhIL-7 (50 ng ml^{-1}) in vitro for 72 h. **g**, L-PHA flow cytometry gating on splenic CD4$^+$ T$_N$ cells from young female mice following intraperitoneal injections of isotype control (1.5 μg) or rhIL-7/M25 complex on days 1, 3 and 5. **h**,**i**, Flow cytometric analysis of L-PHA binding, gating on CD4$^+$ T$_N$ cells from the peripheral blood (**h**) or spleen (**i**) of female mice following i.p. injections of either isotype control (1.5 mg) or anti-IL-7 antibody (M25, 1.5 mg) three times a week for 2 weeks. **j**,**k**, Flow cytometric analysis of IL7Rα (**j**) and pSTAT5 (**k**) levels in splenic CD4$^+$ T$_N$ cells following i.p. injections of either isotype control (1.5 mg) or anti-IL-7 antibody (M25, 1.5 mg) three times a week for 4 weeks. Normalized geometric MFI is shown. Each symbol represents a single mouse. *P*-values determined by two-tailed Wilcoxon (**a**,**e**,**f**) Kruskal–Wallis with Dunn's multiple comparisons test (**b**,**g**,**i**), one-tailed Wilcoxon (**c**,**d**) or one-tailed Mann–Whitney (**h**,**j**,**k**). In panel **h**, *P*-values indicate comparison of 12-week-old isotype control group with 82-week-old anti-IL-7 treatment group. Error bars indicate mean ± s.e.m.

Table 1 | Differential expression of IL-7 signaling pathway genes in aging

		Female ($CD4^+$ T_N)		Male ($CD4^+$ T_N)		Female ($CD4^+$ T_{EM})		Male ($CD4^+$ T_{EM})	
Gene symbol	Gene description	Adjusted *P* value	Fold change	Adjusted *P* value	Fold change	Adjusted *P* value	Fold change	Adjusted *P* value	Fold change
Il7r	IL-7 receptor alpha	1.80×10^{-2}	0.6273	7.42×10^{-1}	0.8618	9.52×10^{-1}	0.9778	1.51×10^{-1}	0.6728
Jak3	Janus kinase 3	6.67×10^{-15}	2.6892	1.20×10^{-1}	1.4740	2.40×10^{-1}	1.3606	3.41×10^{-1}	1.2346
Socs1	Suppressor of cytokine signaling 1	1.81×10^{-8}	2.6417	9.99×10^{-1}	1.0142	1.49×10^{-3}	1.9095	5.85×10^{-1}	−0.3558
Socs3	Suppressor of cytokine signaling 3	4.49×10^{-21}	5.9106	6.84×10^{-1}	1.8401	1.78×10	6.3359	2.62×10^{-8}	2.9469
Jak1	Janus kinase 1	6.62×10^{-1}	0.7575	9.77×10^{-1}	1.0459	1.64×10^{-1}	0.6826	6.21×10^{-1}	0.7994
Il2rg	IL-2 receptor, gamma chain	7.52×10^{-1}	1.1804	9.49×10^{-1}	1.0542	8.70×10^{-1}	1.0482	7.11×10^{-1}	0.8967
Stat5a	Signal transducer and activator of transcription 5 A	6.36×10^{-1}	1.2806	9.27×10^{-1}	1.1085	8.72×10^{-1}	1.0665	9.35×10^{-1}	1.0502

output, existing T_N cells may enjoy a greater share of available IL-7, leading to increased IL-7 signaling[35]. We thus sought to determine if thymectomy in young female mice could drive N-glycan branching by increasing IL-7 signaling in $CD4^+$ T_N cells. Although thymectomized mice demonstrated a precipitous drop in $CD4^+$ T_N cells, neither IL7Rα protein levels nor N-glycan branching were changed in $CD4^+$ T_N cells (Extended Data Fig. 3a–c). Alternatively, loss of estrogen in old female mice may be responsible for altered IL-7 signaling and may explain the sex-dimorphic increase in branching. Indeed, ovariectomy has been shown to increase IL-7 levels in bone marrow[36]. Ovariectomy of young female mice resulted in a small reduction in IL7Rα levels (around 15%) on $CD4^+$ T_N cells at 4 weeks postsurgery (Extended Data Fig. 3d). However, N-glycan branching levels remained unchanged (Extended Data Fig. 3e). Furthermore, branching levels did not change for up to 18 weeks postovariectomy and IL7Rα levels on $CD4^+$ T_N cells remained reduced by only around 15% when measured at 23 weeks postovariectomy (Extended Data Fig. 3f,g). As $CD4^+$ T_N cells from old female mice demonstrated a reduction in IL7Rα levels of around 50% (Fig. 2c and Extended Data Fig. 2g), the decrease of about 15% in IL7Rα induced by ovariectomy may be insufficient to alter branching. To test whether the combined loss of estrogen and thymic output may be required, we examined mice that were both thymectomized and ovariectomized. Similar to ovariectomy alone, these mice demonstrated a small (15%) decrease in IL7Rα levels on $CD4^+$ T_N cells but no change in branching (Extended Data Fig. 3h,i). These data demonstrate that ovariectomy and thymectomy of young female mice, in isolation or in combination, is insufficient to drive increases in N-glycan branching on $CD4^+$ T_N cells. In summary, the IL-7 driven enhancement of N-glycan branching in T_N cells of old female mice appears largely independent of age-associated thymic involution and/or complete loss of ovarian function.

Elevated N-glycan branching in old T cells suppresses function. Age-dependent increases in N-glycan branching are expected to limit TCR-induced activation and proinflammatory responses in old T cells[12–14,16–18]. To initially assess this, we compared induction of the T cell activation marker CD69 in response to anti-CD3 stimulation. Indeed, $CD4^+$ T cells from aged female mice were hyporeactive in comparison with young $CD4^+$ T cells (Fig. 3a). This effect was reversed by treating T cells with the mannosidase I inhibitor kifunensine (KIF), which blocks N-glycan branching[18] (Fig. 3a). To confirm this using a genetic model, we examined aged mice with T cell specific deficiency of the Mgat2 branching enzyme (*Mgat2*$^{fl/fl}$*lck-cre* mice). T cells lacking *Mgat2* have reduced N-glycan branching and show hybrid N-glycans with a single branch extended by poly N-acetyllactosamine[18] (Extended Data Fig. 4a). Indeed, old Mgat2-deficient $CD4^+$ T cells showed enhanced induction of CD69 (Fig. 3b). Consistent with this data, T cell proliferation in old female $CD4^+$ T cells was also rejuvenated by decreasing branching with KIF or *Mgat2* deficiency (Fig. 3c). To confirm that reversing the increase in branching improves TCR signaling specifically in $CD4^+$ T_N cells, we examined the proximal TCR signaling pathway by phosphoflow cytometry of anti-CD3 antibody stimulated splenocytes with gating on the $CD4^+$ T_N pool. Dose-dependent increases in phosphorylation of ERK1/2, Zap70 and CD3-zeta were all significantly attenuated in old relative to young female $CD4^+$ T_N cells (Fig. 3d–f). However, modestly reducing branching in old female $CD4^+$ T_N cells by around 20%, via a 24 h preincubation with KIF (Extended Data Fig. 4b), readily rejuvenated the activation of ERK1/2, Zap70 and CD3-zeta in old female $CD4^+$ T_N cells (Fig. 3d–f). Moreover, phospho-ERK1/2 induction was also increased significantly by *Mgat2* deficiency in $CD4^+$ T_N cells (Extended Data Fig. 4c). Together, these data demonstrate that age-dependent elevation in branching functions to reduce TCR signaling thresholds in old $CD4^+$ T_N cells.

N-glycan branching also suppresses inflammatory T cell responses by both inhibiting proinflammatory T_H17 while promoting anti-inflammatory Treg differentiation[12,37]. Thus, age-dependent increases in N-glycan branching are expected to reduce T cell inflammatory responses in old adults. Indeed, blocking age-associated increases in N-glycan branching in old female $CD4^+$ T cells with either KIF or *Mgat2* deletion enhanced T_H17 differentiation while decreasing Treg induction (Extended Data Fig. 4d,e). Together, these results indicate that aging-induced increases in N-glycan branching functionally suppress proinflammatory T cell activity.

Elevated N-glycan branching suppresses immunity in old mice. In immune-competent hosts, nontyphoidal *Salmonella* (NTS) infection induces a robust T_H17 response and a localized self-limited infection in the gut mucosa[38,39]. However in old adults, NTS infection is a frequent cause of bacteremia[40], as the pathogen disseminates from the gut to systemic sites, a process that can be recapitulated in the mouse[41]. Prior studies have shown that T_H17 responses are critical to limit NTS dissemination from the gut[42,43]. Therefore, we sought to investigate whether the age-associated increases in N-glycan branching suppress T cell function in vivo, by employing an infectious colitis model with one of the most prevalent NTS serovar, *Salmonella enterica* serovar Typhimurium (*S.* Typhimurium). We infected old wild-type female mice with a virulent strain of *S.* Typhimurium after streptomycin pretreatment, as previously described[42]. This resulted in two deaths and high levels of *S.* Typhimurium recovered from the Peyer's patches, the mesenteric

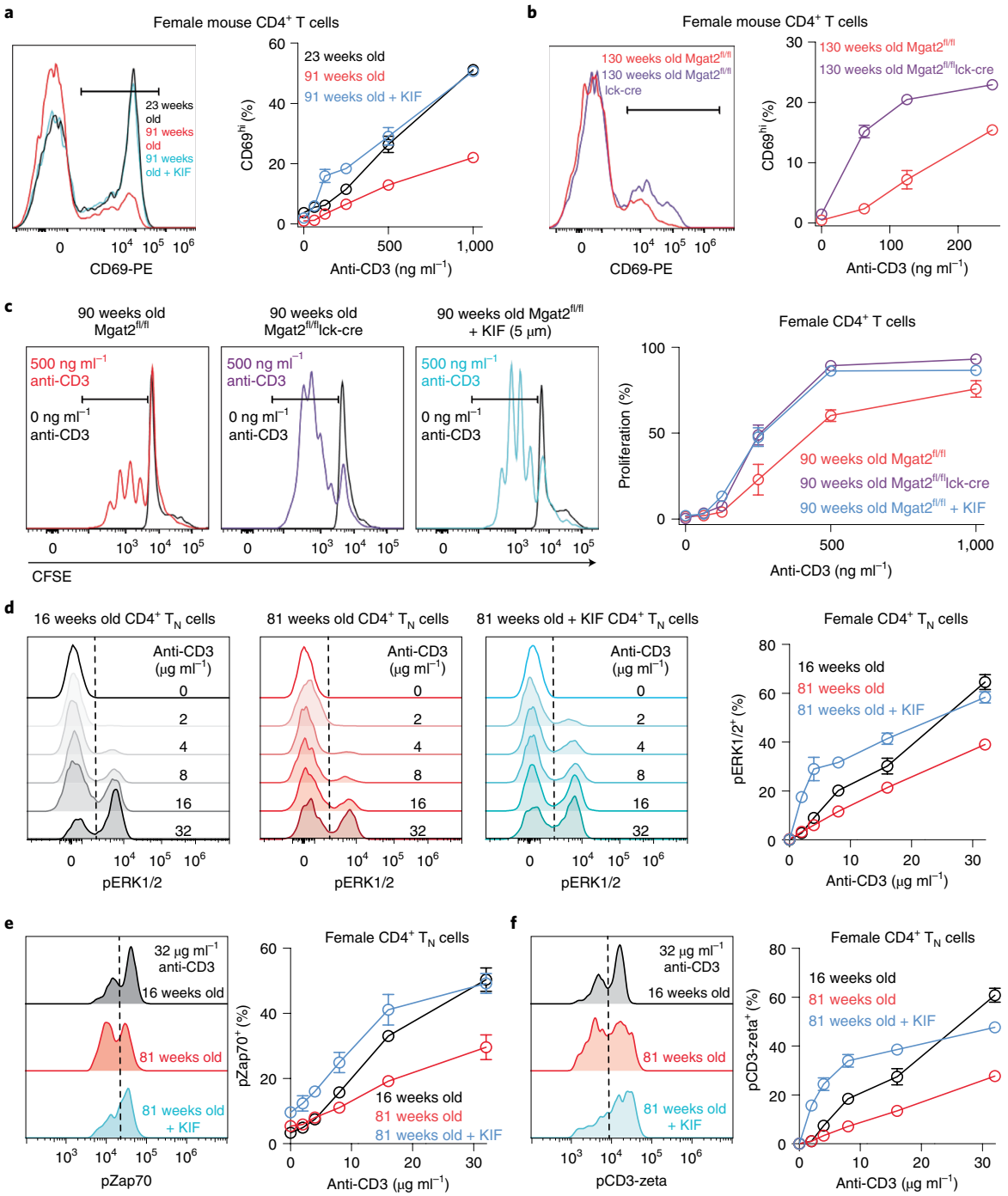

Fig. 3 | Age-dependent increases in N-glycan branching suppress T cell function in female mice. a, Splenocytes from wild type female mice of the indicated ages were activated with plate-bound anti-CD3e for 24 h in the presence or absence of 5 μM KIF. Total CD4+ T cells were analyzed for CD69 expression by flow cytometry. **b**, CD69 expression was analyzed as in (**a**), comparing CD4+ T cells from old female mice with and without T cell specific *Mgat2 deficiency*, gating additionally on L-PHA negative cells in *Mgat2*$^{fl/fl}$*/lck-cre* mice. **c**, Splenocytes from female mice of the indicated ages and genotypes were activated with plate-bound anti-CD3e for 72 h in the presence or absence of 5 μM KIF. Total CD4+ T cells were analyzed for CFSE dilution by flow cytometry. **d**–**f**, Splenocytes from female mice of the indicated ages were pretreated with or without KIF for 24 h, followed by activation with plate-bound anti-CD3e for 15 min. Following fixation and permeabilization, phospho-ERK (**d**), phospho-Zap70 (**e**) or phospho-CD3-zeta (**f**) induction was analyzed in CD4+ T_N cells by flow cytometry. Data are representative of at least three independent experiments. Error bars indicate mean ± s.e.m.

lymph nodes (MLN) and the spleen, consistent with the pathogen's dissemination from the gut to systemic sites (Fig. 4a–c). In contrast, infecting age-matched T cell specific *Mgat2*-deficient female mice in parallel (that is, *Mgat2*$^{fl/fl}$*lck-cre*) resulted in no deaths and reduced colonization of Peyer's patches, MLN and the spleen (Fig. 4a–c). *S.* Typhimurium colonization of the cecal content did not differ between control and *Mgat2*-deficient old female mice (Extended Data Fig. 4f). Infected *Mgat2* deficient old female mice also showed increased IL-17+ and reduced FoxP3+ cells in the bowel compared with infected controls (Fig. 4d,e), consistent with our in vitro data that age-dependent increases in N-glycan branching suppresses T_H17 and enhances Treg responses. Collectively, these data indicate

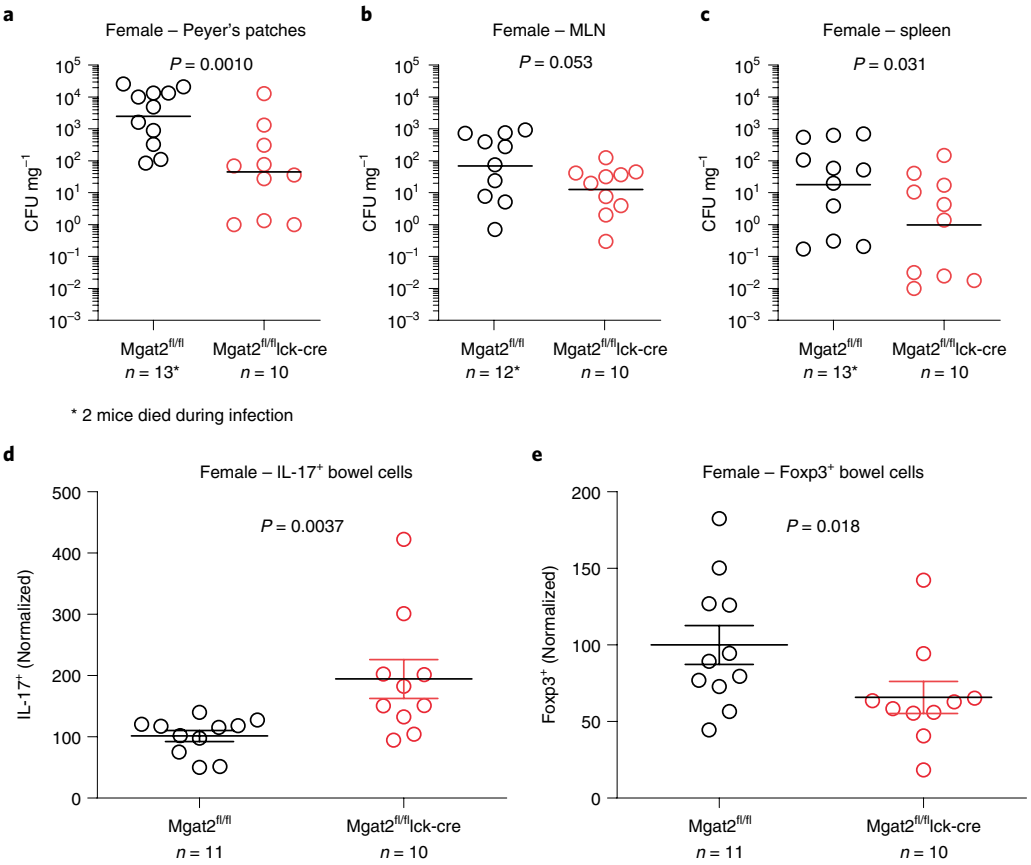

Fig. 4 | Elevated N-glycan branching in T cells suppresses immune response to *Salmonella* in old female mice. a–e, *Mgat2*$^{fl/fl}$ and *Mgat2*$^{fl/fl}$*lck-cre* female mice were pretreated with streptomycin intragastrically 1 day before inoculation with *S.* Typhimurium (5×10^8 CFU per mouse). CFU in Peyer's patches (**a**), MLN (**b**) and spleen (**c**) were enumerated 72 h after infection. Total IL-17$^+$ (**d**) and Foxp3$^+$ (**e**) cells in the gut were detected by flow cytometry and normalized to the average number of cells from *Mgat2*$^{fl/fl}$ mice. Each symbol represents a single mouse. *P*-values by one-tailed Mann–Whitney. Bars, geometric mean (**a–c**) or mean ± s.e.m. (**d**, **e**).

that age-dependent increases in N-glycan branching in female T cells promotes *S.* Typhimurium dissemination.

N-glycan branching is elevated in old human female T cells. To investigate whether N-glycan branching is similarly elevated with aging in humans, we examined females and males ranging in age from 19 to 98 years old. Humans showed a similar phenotype as mice, with age-dependent increases of N-glycan branching in the following order: CD4$^+$ T cells > CD8$^+$ T cells > B cells, females > males and T_N > memory T cells (Fig. 5a–e and Extended Data Fig. 5a–d). Branching in CD45RA$^+$CD45RO$^-$CD4$^+$ T_N cells demonstrated a Gaussian shift of the entire population, indicating that subset heterogeneity is not responsible for the observed increase (Fig. 5a). Restricting analysis to ages from 19 to 65 years showed similar results in female CD4$^+$ T_N cells, demonstrating that the data are not significantly skewed by those over 90 years old (Extended Data Fig. 5e,f). As with mice, we examined whether cell-intrinsic and/or cell-extrinsic factors were driving the age-associated increase in N-glycan branching. Indeed, normalizing cell-extrinsic factors by resting peripheral blood mononuclear cells (PBMCs) in culture for 4 days resulted in a significant decrease in age-associated differences in branching in CD4$^+$ T_N cells (Extended Data Fig. 5g).

IL-7 and GlcNAc synergistically raise branching in old human T_n cells. As in mice, IL-7 signaling downregulates IL7Rα expression in human T cells[44,45]. Furthermore, IL7Rα levels have been reported to decrease in human T_N cells with age, suggesting that IL-7 signaling increases with age[46,47]. We previously reported that short-term in vitro treatment of resting human CD4$^+$ T cells (mixed naive and memory) for 3 days with IL-7 lowers branching[17], which is opposite to effects on mouse CD4$^+$ T_N cells described above. However, this analysis was agnostic to gender and naive versus memory cells. We repeated these experiments but specifically analyzed resting female CD4$^+$ T_N and CD8$^+$ T_N cells and increased exposure to IL-7 to 9 days, the latter to better reflect long term exposure in vivo. This revealed that exogenous IL-7 induced a small but statistically significant increase in N-glycan branching in T_{EM} cells, but was insufficient to increase branching in T_N cells (Fig. 6a,b and Extended Data Fig. 6a,b).

IL-7 regulates mRNA expression of *Mgat1* in human T cells, where increased activity can either raise or lower branching depending on metabolic supply of UDP-GlcNAc substrate to the Golgi branching enzymes[17]. The Mgat1, 2, 4 and 5 branching enzymes all use UDP-GlcNAc as a donor substrate, but with declining efficiency (Extended Data Fig. 1a). The K_m of Mgat4 and -5 for UDP-GlcNAc is around 100- to 200-fold worse than that of Mgat1 (~0.04 mM). Thus, when UDP-GlcNAc is limiting, elevated Mgat1 activity paradoxically lowers branching by outcompeting Mgat4 and -5 for their common substrate. However, with higher UDP-GlcNAc levels, Mgat5 activity is not limited, and increased Mgat1 expression enhances branching, as would be expected[17]. This suggests that, in humans, IL-7 induced increases in Mgat1 activity may synergize with an age-dependent increase in UDP-GlcNAc.

UDP-GlcNAc biosynthesis by the hexosamine pathway is inhibited metabolically by aerobic glycolysis and glutaminolysis via inhibition of de novo synthesis from glucose but increased by

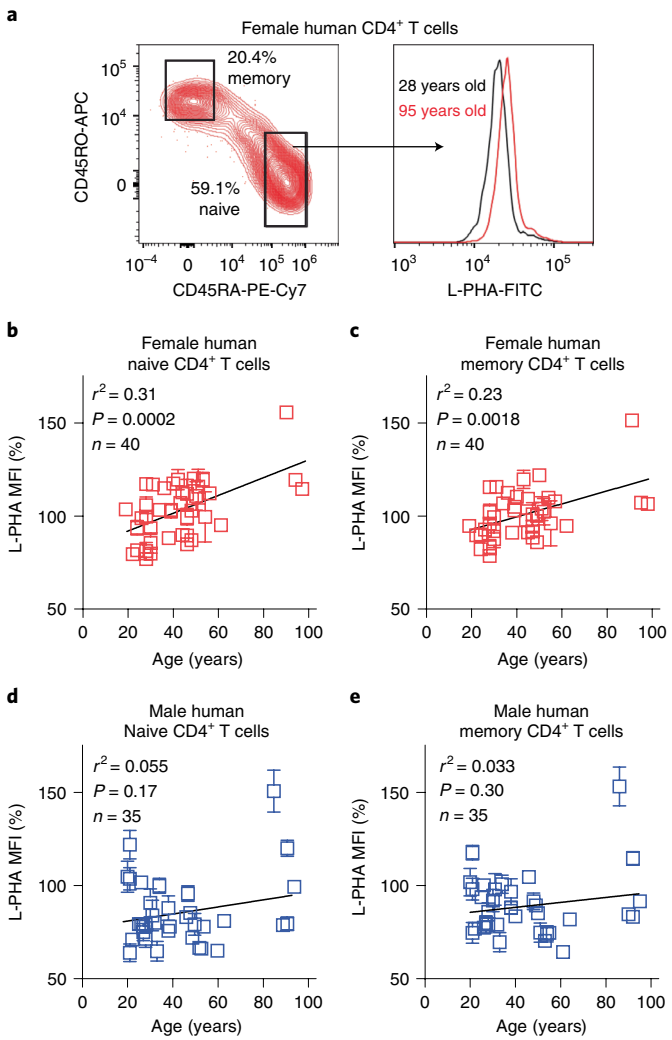

Fig. 5 | N-glycan branching increases with age in human T cells. a, A representative flow cytometry plot gated on CD4+ T cell is shown (left), demonstrating gating on naive (CD45RA+CD45RO−) and memory (CD45RA−CD45RO+) subsets. Also shown are representative L-PHA histograms (right) of young and old CD4+ T_N cells, demonstrating elevated L-PHA binding in older females. **b**,**c**, Female PBMCs of the indicated ages were measured for L-PHA binding by flow cytometry gating on naive CD4+ T cells (**b**) or memory CD4+ T cells (**c**). **d**,**e**, Male PBMCs of the indicated ages were measured for L-PHA binding by flow cytometry, gating on naive CD4+ T cells (**d**) or memory CD4+ T cells (**e**). Data were normalized to a reference control across experiments. Each symbol represents a single individual. R^2 and *P*-values by linear regression. Error bars indicate mean ± s.e.m.

salvage of N-acetylglucosamine (GlcNAc)[12,16,29]. Supplementing cells, mice or humans with GlcNAc increases UDP-GlcNAc levels and N-glycan branching in activated more than in resting T cells[12,16,17,24,29]. Interestingly, using targeted liquid chromatography–tandem mass-spectrometry (LC-MS/MS) to assess GlcNAc and its stereoisomers (N-acetylhexosamines or HexNAc) in human serum revealed marked increases with age in both females and males (Fig. 6c,d)[48,49]. However, endogenous serum HexNAc levels correlated positively with N-glycan branching in CD4+ T_N cells of females but not of males (Fig. 6e,f), paralleling the age-dependent increase in N-glycan branching being greater in females. In contrast, HexNAc levels in old female mice were not elevated significantly compared with young female mice (Extended Data Fig. 6c), consistent with the greater direct effect of IL-7 on branching in mouse CD4+ T_N cells. Consistent with IL-7 raising Mgat1 levels, coincubating resting human female PBMCs with GlcNAc plus IL-7 for 9 days synergistically increased N-glycan branching in CD4+ T_N cells (Fig. 6a,b), while having only an additive effect in CD4+ T_{EM} cells (Extended Data Fig. 6a,b). Together, these data suggest that, in humans, elevated IL-7 signaling in T_N cells synergizes with age-dependent increases in serum GlcNAc to raise N-glycan branching in the following order: naive> memory and female > male T cells.

As with mice, the age-dependent elevation in N-glycan branching also suppressed T cell activity, as treating old human female PBMCs with KIF to inhibit branching rejuvenated ligand-induced T cell activation and proliferation (Extended Data Fig. 6d,e). Reduced pERK levels in response to TCR stimulation are among the few functional defects attributed specifically to old human CD4+ T_N cells[2,11]. To confirm that reversing the increase in branching improves TCR signaling specifically in CD4+ T_N cells, old female PBMCs were pretreated with or without KIF for 24 h to establish a ~15% reduction in L-PHA staining (Extended Data Fig. 6f,g). They were then stimulated with anti-CD3 for 15 min before analysis of pERK levels by flow cytometry, gating specifically on CD4+ T_N cells. Despite the small reversal in branching levels, KIF treatment significantly increased intracellular pERK levels, demonstrating that the age-associated increase in N-glycan branching acts to limit human CD4+ T_N cell function (Fig. 6g).

Discussion

Our data reveal that human aging-associated increases in serum GlcNAc synergize with elevated IL-7 signaling to upregulate N-glycan branching and thereby induce hypo-activity of female greater than male naive T cells. Our data also suggests an example of antagonistic pleiotropy, where a trait that is beneficial early becomes harmful later in life. IL-7 signaling is a critical mediator of peripheral T cell proliferation and homeostatic maintenance, particularly following loss of thymic output of T_N cells in early adulthood[45]. However, our data suggest that, in later life, excess IL-7 signaling in females greater than males can synergistically combine with age-dependent increases in GlcNAc to limit T_N function via increased branching. Thus, elevated IL-7 signaling may be beneficial through most of human adulthood, but contribute to immunosenescence in old females more than in old males secondary to rising GlcNAc. Consistent with this hypothesis, reduced IL7Rα expression—a marker of elevated IL-7 signaling in humans[44,45]—correlates with healthy aging and reduced immune related disorders in middle-age, yet also with decreased survival among both the middle-aged and nonagenarians[50].

Early reports of T cell hyporeactivity in older adults used mixed populations. In analyses of distinct T cell subsets, functional defects have persisted in CD4+ T_N cells but have been brought into question for other subsets[2,11]. Interestingly, this pattern parallels the magnitude of N-glycan branching observed in this study, which are in the order CD4+ > CD8+ and T_N > T_{EM}. As age-induced increases in N-glycan branching are reversed by cell culture, in vitro studies lasting days will underestimate the true extent of functional impairment. In this regard, in vivo studies and short-term in vitro signaling assays will probably be more accurate.

Elevated IL-7 signaling was observed in female more than in male CD4+ T_N cells but not in CD4+ T_{EM} cells. Moreover, exogenous IL-7 similarly raised branching in both male and female CD4+ T_N cells regardless of age. This indicates that, rather than a wholescale increase in IL-7 availability, cell-extrinsic differences in IL-7 signaling specific to T_N cells in females compared with males primarily drives the age-dependent increase in branching. As ovariectomy in mice did not enhance branching, the sex difference seems to be driven by sex chromosomes rather than female sex hormones. However, as ovariectomy also blocks androgens and other factors secreted by postmenopausal ovaries[51], a role for other secreted

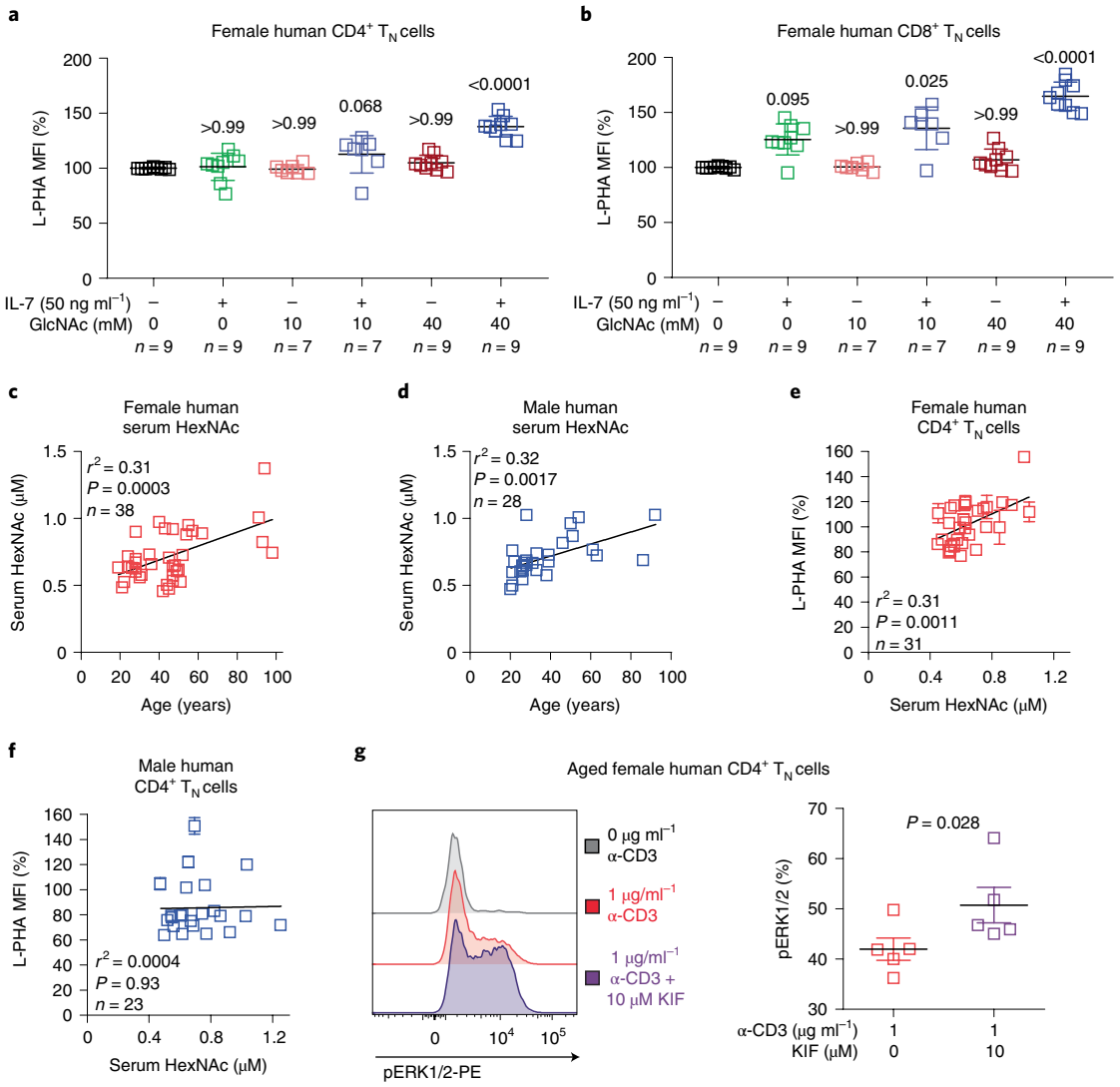

Fig. 6 | Serum N-acetylglucosamine increases with age and synergizes with IL-7 to raise N-glycan branching in human T cells. a,**b**, PBMCs from healthy female donors (28–45 years old) were cultured with or without rhIL-7 (50 ng ml^{-1}) and/or GlcNAc (10 mM or 40 mM) for 9 days, then analyzed for L-PHA binding by flow cytometry, gating on CD4$^+$ T_N cells (**a**) or CD8$^+$ T_N cells (**b**). **c**,**d**, Human serum from healthy female (**c**, 19–98 years old; 45 ± 20 years old) or male (**d**, 20–92 years old; 38 ± 19 years old) donors of the indicated ages was analyzed for HexNAc levels by LC-MS/MS. **e**,**f**, Correlation of serum HexNAc with L-PHA binding on CD4$^+$ T_N cells in healthy female (**e**, 19–98 years old; 44 ± 20 years old) or male (**f**, 20–92 years old; 40 ± 20 years old) donors. **g**, Flow cytometric analysis of intracellular pERK1/2 in 90- to 94-year-old female human CD4$^+$ T_N cells stimulated with plate-bound anti-CD3 for 15 min. Cells were pretreated with or without 10 μM KIF for 24 h before stimulation. Each symbol represents a single individual. Normalized geometric MFI is shown (**a**,**b**,**e**,**f**). *P*-values by Kruskal–Wallis with Dunn's multiple comparisons test (**a**,**b**), linear regression (**c**–**f**), and one-tailed Mann–Whitney (**g**). Error bars indicate mean ± s.e.m.

factors cannot be excluded. As there are several immune specific genes on the X chromosome, an effect of sex chromosomes could arise through incomplete X-inactivation of a gene(s) that regulates branching and survival of T_N cells. Indeed, our RNA-seq data identified several genes located on the X chromosome with altered gene expression in old female but not male CD4$^+$ T_N cells.

Though previous studies have examined transcriptome changes in highly purified aged T cell subsets[52], we analyzed T cell populations by age and sex. Among the relatively few DEGs identified between young versus old CD4$^+$ T_N cells, less than 30% of these overlapped between males and females, suggesting sex-specific differences in T_N cell aging. Male-female differences in immune function are well described, such as the increased risk of many autoimmune diseases in females[53] and sex differences in morbidity and mortality with regard to SARS-CoV-2[54,55]. However, these sex differences can be mitigated or reversed in older adults. For example, onset of the autoimmune disease relapsing-remitting multiple sclerosis typically occurs in young adults (mean onset of age around 30 years) with a 3:1 ratio of females to males, but is only 1.5:1 in those who develop disease aged over 65 years[56]. Moreover, while immune responses to vaccination are consistently higher in females than males throughout childhood and adulthood, this trend is reversed in aged individuals for the pneumococcal and Td/Tdap vaccines[57]. Furthermore, although females demonstrate higher antibody responses to influenza vaccination throughout life and in old age, old males produce higher avidity antibodies than old females indicating reduced T cell help in old females[58]. These reversals are consistent with the sex-dimorphic increase in N-glycan branching in older adults and imply that effective interventions of immune senescence may require sex-specific strategies.

Our data provide several potential therapeutic targets in T cell aging. First, the N-glycan branching pathway has known pharmacological inhibitors that have undergone human testing[59]. Although chronic use of these agents may be toxic, short-term treatment during acute infection or at the time of vaccination may have benefit with limited toxicity. Development of T cell targeted strategies or novel inhibitors with better toxicity profiles are also attractive pursuits. Second, although IL-7 agonists have been explored extensively, our data suggest that this will lead to impaired T_N cell function via increased branching. Rather, co-administration of an IL-7 agonist with N-glycan antagonists should promote maintenance of the T_N cell pool while also ensuring that they are functional. Finally, reversing the elevation in serum GlcNAc either by limiting production, promoting metabolism/excretion or selective depletion may be an effective means of reversing T cell aging alone or in combination with IL-7 targeting agents.

Methods

Mice. All mouse experiments used C57BL/6 mice. C57BL/6 *Mgat2*$^{f/f}$ and *Mgat2*$^{f/f}$Lck-Cre were bred inhouse by initially crossing *Mgat2*$^{f/f}$ (JAX, catalog no. 006892) and Lck-Cre (JAX, catalog no. 003802) mice and are previously described[27]. Young and aged wild-type C57BL/6 mice were obtained from the National Institute of Aging (NIA) colony maintained at Charles River Laboratories. *Cd45.1* (JAX, catalog no. 002014) C57BL/6 mice were obtained from JAX. C57BL/6 mice were ovariectomized, thymectomized, ovariectomized and thymectomized, or subject to sham surgery by JAX surgical services at 9 weeks of age. For all experiments, delivered animals were allowed to acclimate to our vivarium for at least 1 week before measurements or the start of experiments. Mice were housed at the University of California. Irvine in an environment-controlled, pathogen-free barrier facility on a 12-h/12-h light/dark cycle at constant temperature and humidity, with food and water available ad libitum. Young mice were 7–32 weeks old, while old mice were 74–130 weeks old. Age and sex information for particular experiments is indicated in the figures and/or figure legends. To acquire mouse plasma, blood was collected in sterile tubes containing 0.1 M EDTA as an anticoagulant. The Institutional Animal Care and Use Committee of the University of California, Irvine, approved all mouse experiments and protocols (protocol number AUP-19-157).

Human subjects. Male and female subjects with an age range of 19–98 years old were examined in this study. Age and sex for particular experiments are indicated in the figures and/or figure legends. Individuals with cancer, uncontrolled medical disease or any other inflammatory syndrome were excluded. Human whole blood was collected from healthy individuals through the Research Blood Donor Program serviced by the Institute for Clinical and Translational Science (ICTS) or through The 90+ Study at the University of California, Irvine. All procedures with human subjects were approved by the Institutional Review Board of the University of California, Irvine. All study participants gave written informed consent and were uncompensated.

T cell isolation and culture. For ex vivo and in vitro mouse experiments, erythrocytes were depleted from splenic or lymph node cell suspensions by incubation with red blood cell (RBC) lysis buffer followed by negative selection using EasySep naive CD4$^+$ T Cell Isolation Kit or EasySep CD4$^+$ T Cell Isolation Kit (STEMCELL Technologies) according to the manufacturer's instructions and supplemented with or without 20 μg ml^{-1} biotinylated L-PHA (Vector Labs) to deplete non-*Mgat2* deleted cells. Freshly harvested cells were cultured (2×10^5–5×10^6 cells) in RPMI-1640 (Thermo Fisher Scientific) supplemented with 10% heat inactivated fetal bovine serum (Sigma-Aldrich), 2 μM L-glutamine (Gibco), 100 U ml^{-1} penicillin/streptomycin (Gibco), and 50 μM β-mercaptoethanol (Gibco) as previously described[14,16,27]. Human PBMCs isolated by density gradient centrifugation over Histopaque-1077 (Sigma-Aldrich) or Lymphoprep (StemCell Technologies) were stimulated with plate-bound anti-CD3 (OKT3, eBioscience) plus soluble anti-CD28 (CD28.2, eBioscience) in medium as described above. PBMCs were pretreated with or without 5–10 μM KIF 24 h before stimulation if indicated. For pharmacological treatments, cells were incubated with GlcNAc (40 mM added daily, Wellesley Therapeutics), KIF (5–10 μM, Glycosyn), recombinant human IL-7 (50 ng ml^{-1} in vitro; 0.5 μg–1.5 μg in vivo, R&D Systems), and/or anti-mouse/human IL-7 antibody (clone M25; 5–15 μg, BioXCell) as indicated[60]. We induced T_H17 and iTreg as previously described[12].

Flow cytometry. We performed flow cytometry experiments as previously described[14,27]. Depending on cell yields and number of experimental conditions, we performed cell staining in two to four replicates. Mouse antibodies for surface, intracellular and phosphoflow staining to CD69 (H1.2F3), IL-17 (eBio17B7), CD4 (RM4−5), CD8α (53-6.7), CD19 (1D3), Foxp3 (Fjk-16s), CD44 (IM7), CD62L (MEL-14), CD3 (145−2C11 and 17A2), CD25 (PC61.5), IL7Rα (A7R34), Rat IgG2a kappa Isotype Control (eBR2a), phospho-STAT5 (SRBCZX), phospho-CD247 (3ZBR4S), phospho-Zap70 (n3kobu5) and Mouse IgG1 kappa Isotype Control (P3.6.2.8.1) were purchased from eBioscience/Thermo Fisher Scientific. In addition, antibodies to phospho-ERK1/2 (MILAN8R), CD45RA (HI100), CD4 (RM4-5), CCR7 (4B12), CD25 (BC96) and CD19 (HIB19) were purchased for human cells. Antibodies to mouse CD45.1 (A20), CD45.2 (104), phospho-ERK1/2(4B11B69) and anti-human CD45RO (UCHL1) and CD8 (SK1) were purchased from BioLegend. All antibodies were used at manufacturer recommended dilutions for flow cytometry. DyLight 649-conjugated Streptavidin, fluorescein labeled ConA and both fluorescein labeled and biotinylated L-PHA were purchased from Vector Labs. Proliferation was assessed by staining cells with a CellTrace 5,6-carboxyfluorescein diacetate succinimidyl ester (CFSE) proliferation kit (Thermo Fisher Scientific). We performed flow cytometry experiments with the BD FACSAria Fusion Sorter, LSR II, Invitrogen Attune NxT Flow Cytometer or ACEA Novocyte Flow Cytometer and analyzed data following appropriate compensation using FlowJo software. The gating strategy used is demonstrated for CD4$^+$ T_N cells (Extended Data Fig. 1b).

Anti-CD3 stimulation and phosphoflow cytometry. Tissue-culture-treated flat-bottom 96-well plates were coated with the indicated concentrations of functional grade anti-CD3e (anti-mouse clone 145-2C11; anti-human clone OKT3) in 100 μl of PBS per well and incubated at 37 °C for 3 h or 4 °C overnight. The anti-CD3 solution was then aspirated and replaced with 150 μl of cells in complete medium at 2×10^6 cells per milliliter for human PBMCs or 6×10^6 cells per milliliter for mouse splenocytes. Plates were then centrifuged at 250 relative centrifugal force for 2 min to bring cells in contact with the bottom of the wells and incubated in a tissue-culture incubator for 15 min. Cells were fixed by directly adding 100 μl per well of 4% PFA, then resuspended, transferred to round-bottom plates, and incubated at 37 °C for 15 min. For human PBMCs, cells were then permeabilized by resuspending in 200 μl of ice-cold methanol, followed by sealing the plate and vortexing vigorously. Cells were left in methanol overnight at 4 °C, before washing and staining in routine FACS buffer. For mouse splenocytes, cells were permeabilized with 200 μl of intracellular staining permeabilization wash buffer (Biolegend, catalog no. 421002) instead of methanol and stained using this buffer instead of routine FACS buffer. Data was collected on an ACEA Novocyte Flow Cytometer or Invitrogen Attune NxT Flow Cytometer and analyzed following appropriate compensation using FlowJo software.

Mouse *Salmonella* experiments. Mice were pretreated with streptomycin (0.1 ml of a 200 mg ml^{-1} solution in sterile water) intragastrically 1 day before mock-infection or inoculation with *S.* Typhimurium strain IR715—a nalidixic acid-resistant derivative of ATCC 14028s (5×10^8 colony forming units (CFU) per animal). At 72 h after infection, mice were euthanized and the cecal content, Peyer's patches, MLN and spleen were collected for enumerating bacterial CFU through serial tenfold dilutions plated on agar plates. Additionally, intestinal cells were isolated from around one-third of the cecum and the entire colon by first cutting the cylindrical tissue lengthwise and cleaning the tissue of fecal matter by vigorously shaking the tissue in cold wash buffer (HBSS, 15 mM HEPES, 1% antibiotic/antimycotic (Ab/Am)). The intestinal segments were cut into 3–5 mm pieces on ice and placed into gentleMACS C tubes (Miltenyi Biotec) with 10 ml of prewarmed (37 °C) HBSS containing 10% FBS, 15 mM HEPES, 5 mM EDTA and 1% Ab/Am, and run twice on a GentleMACS dissociator (Miltenyi Biotec) using program m_spleen_04, incubated in a shaking water bath for 10 min, then centrifuged at 720*g* for 2 min. The supernatant containing intraepithelial cells was removed and placed on ice. The remaining tissue with lamina propria cells was washed with 30 ml ice-cold IMDM solution containing 10% FBS and 1% Ab/Am then resuspended in a 10 ml mixture of Liberase (20 μg ml^{-1}) and Collagenase (1 mg ml^{-1}) in prewarmed IMDM solution shaken at 37 °C for 45 min. The digested tissues were placed in C tubes and underwent program B and m_spleen_04 on the GentleMACS dissociator. Afterwards, both the supernatant containing intraepithelial cells and the digested tissue containing lamina propria cells were further purified via Percoll gradient 40% on 80%, strained through a 70 μm cell strainer (BD Biosciences) and pooled in IMDM solution for analysis of bowel cells.

Mouse adoptive transfer and IL-7 experiments. Lymphocytes were prepared from pooled inguinal lymph nodes and splenocytes and purified for naive CD4$^+$ T cells from CD45.2 C56BL/6 donor mice as described above then injected intravenously by tail vein in 200 μl of PBS into CD45.1 congenic C57BL/6 recipient mice. For in vivo IL-7 treatment, mice were injected intraperitoneally (i.p.) with either 200 μl of PBS or rhIL-7/M25 cytokine/antibody complex (R&D Systems and BioXCell) every 2 days. Before injection, the cytokine/antibody complex were generated through coincubation for 30 mins at room temperature. For IL-7 blockade experiments, mice were injected i.p. with 1–1.5 mg of Mouse IgG1 isotype control antibody (MOPC-21, BioXCell) or anti-mouse/human IL-7 (M25, BioXCell) in 200 μl of PBS three times at 2-day intervals per week as indicated.

RNA extraction, library preparation and sequencing. Cell suspensions were prepared from pooled lymph nodes (axillary, brachial, cervical and

inguinal) and splenocytes, and then purified for $CD4^+$ T cells through negative selection using an EasySep $CD4^+$ T cell Isolation Kit (STEMCELL Technologies). Cell suspensions were then stained and FACS-sorted for either naive($CD3^+CD4^+CD25^-CD62L^+CD44^-$) or effector memory ($CD3^+CD4^+CD25^-CD62L^-CD44^+$) populations by BD FACSAria Fusion Sorter. Three biological replicates each with representative levels of N-glycan branching were obtained for young female $CD4^+$ T_N, old female $CD4^+$ T_N, young male $CD4^+$ T_N, old male $CD4^+$ T_N, young female $CD4^+$ T_{EM}, old female $CD4^+$ T_{EM}, young male $CD4^+$ T_{EM} and old male $CD4^+$ T_{EM}.

Total RNA was then isolated using an RNeasy Plus Micro Kit (Qiagen) and analyzed for RNA integrity number (RIN) with an Agilent Bioanalyzer 2100. RIN of all samples was determined to be ≥9.0. Subsequently, 125 ng of total RNA was used for library preparation through the NEBNext Poly(A) mRNA Magnetic Isolation Module before using NEBNext Ultra II DNA Library Prep Kit for Illumina. Collected samples were cleaned with AMPure XP beads (Beckman Coulter) to make RNA into strand-specific cDNA libraries with multiplexing barcodes from NEBNext Multiplex Oligos for Illumina (Index Primer Sets 1 and 2). RNA-seq libraries were then analyzed by qPCR (KAPA Biosystem), normalized to 2 nM and pooled for multiplexing in equal volumes, then underwent a paired-end 100-bp sequencing run on a HiSeq 4000 (Illumina).

The quality of the sequencing was first assessed using fastQC tool (v.0.11.2). Raw reads were then adapter- and quality trimmed and filtered by a length of 20 bases using trimmomatic (v.0.35). Trimmed reads were mapped to the mouse mm10 reference genome using a splice aware aligner Tophat2 (v.2.1.0) and resulting BAM files were processed using Samtools (v.1.3), and gene expression was quantified with featureCounts (subread v.2.0.1, featureCounts v.1.5.0–p3) as raw counts and cufflinks (v.2.2.1) as FPKM (fragments per kilo base of transcript per million mapped fragments) values. Raw counts were normalized and differential analysis was done using R package DESeq2 (v.1.22.2) with a false discovery rate (FDR) cut off at 0.05. The associated analytical scripts can be found using the following link: https://github.com/ucightf/demetriou. A multidimensional scaling plot was generated using limma (v.3.38.3).

LC-MS/MS analysis. Human serum samples for metabolomics analysis were prepared as described previously[48]. Metabolites from 50 µl of serum were extracted by the addition of 200 µl of ice-cold extraction solvent (40% acetonitrile, 40% methanol and 20% water). Thereafter, the samples were shaken at 4 °C for 1 h at 1,400 rpm in a Thermomixer R (Eppendorf) and then centrifuged at 4 °C for 10 min at ~18,000*g* in an Eppendorf microcentrifuge. The supernatant was transferred to fresh tubes and evaporated in a Speedvac (Acid-Resistant CentriVap Vacuum Concentrators, Labconco). The dry-extract samples were stored at −80 °C. The dry eluted metabolites were resuspended in 100 µl of water containing internal standards D^7-glucose at 0.2 mg ml^{-1} and H-tyrosine at 0.02 mg ml^{-1}. Eluted metabolites were analyzed in negative mode at the optimal polarity in multiple reaction monitoring mode on an electrospray ionization triple-quadrupole mass spectrometer (AB Sciex 4000Qtrap). Standard curves were prepared by adding increasing concentrations of GlcNAc or N-Acetyl-D-[UL-$^{13}C_6$]glucosamine (Omicron Biochemicals) to a 50 µl aliquot of control serum. Raw data were imported to MultiQuant software (AB Sciex, v.2.1) for peak analysis and manual peak confirmation. The resulting data including area ratio are then exported to Excel.

Statistical analysis. All statistical tests are nonparametric tests, except for Extended Data Fig. 5g, where the Shapiro–Wilk normality test was performed and passed. Data where multiple independent experiments were normalized and combined are analyzed by the Wilcoxon nonparametric paired test. Statistical analyses were calculated with Prism software (GraphPad). P-values were calculated from two/one-tailed Wilcoxon or Mann–Whitney tests unless specified otherwise. Details of tests performed are found in the figure legends. We performed one-tailed tests only when directionality was predicted a priori. No statistical methods were used to predetermine sample sizes, but sample sizes were based on our previous experience performing comparable experiments and were similar to those reported in previous publications[11,18]

Randomization, blinding and data exclusion. Mice and humans were selected and assessed randomly. Mouse littermates were distributed randomly into treatment groups for in vivo experiments. Human participants were enrolled randomly and allocated based on age and gender. As physical attributes of mice are the same, no blinding was performed for mouse experiments. Human subjects were not blinded as this was an observational study rather than a clinical trial. The individuals performing serum measurements were blinded to sex and age. We performed quantification by flow cytometry in a uniform manner for all samples. For all flow cytometry data, nonviable cells and doublets were excluded. In flow cytometry experiments, individual replicates were excluded if fluidics errors such as bubbles or clogging were detected during sample collection and substantially altered scattering characteristics or event counts. In Fig. 2h, one mouse in the '12w.o. Isotype' group died on day 8, likely due to mishandling/misinjection, and could not be included in the 2-week timepoint. In Fig. 4b, one data point in the *Mgat2*$^{fl/fl}$ group could not be included due to failed MLN dissection. Data from experiments where positive and/or negative controls failed were excluded.

Reporting Summary. Further information on research design is available in the Nature Research Reporting Summary linked to this article.

Data availability

RNA-seq data has been deposited with the Gene Expression Omnibus under accession number GSE184496. The mouse 10mm reference genome was obtained from https://hgdownload.soe.ucsc.edu/downloads.html#mouse. Statistical source data is provided for all main and Extended Data Figures in the supplementary information. Additional data that support the findings within this article are available from the corresponding author upon reasonable request.

Code availability

The code for differential analysis of RNA-seq data using R package DESeq2 has been uploaded to a github repository and can be found at https://github.com/ucightf/demetriou.

Received: 24 March 2021; Accepted: 2 February 2022;
Published online: 18 March 2022

References

1. Goronzy, J. J. & Weyand, C. M. Mechanisms underlying T cell ageing. *Nat. Rev. Immunol.* **19**, 573–583 (2019).
2. Nikolich-Zugich, J. The twilight of immunity: emerging concepts in aging of the immune system. *Nat. Immunol.* **19**, 10–19 (2018).
3. Centers for Disease Control and Prevention (CDC). Estimates of deaths associated with seasonal influenza—United States, 1976–2007. *MMWR Morb Mortal Wkly Rep* **59**, 1057–1062 (2010).
4. Wiersinga, W. J., Rhodes, A., Cheng, A. C., Peacock, S. J. & Prescott, H. C. Pathophysiology, transmission, diagnosis, and treatment of coronavirus disease 2019 (COVID-19): a review. *JAMA* **324**, 782–793 (2020).
5. Chen, P. L. et al. Non-typhoidal Salmonella bacteraemia in elderly patients: an increased risk for endovascular infections, osteomyelitis and mortality. *Epidemiol. Infect.* **140**, 2037–2044 (2012).
6. Nichol, K. L., Nordin, J. D., Nelson, D. B., Mullooly, J. P. & Hak, E. Effectiveness of influenza vaccine in the community-dwelling elderly. *N. Engl. J. Med.* **357**, 1373–1381 (2007).
7. Targonski, P. V., Jacobson, R. M. & Poland, G. A. Immunosenescence: role and measurement in influenza vaccine response among the elderly. *Vaccine* **25**, 3066–3069 (2007).
8. Carrette, F. & Surh, C. D. IL-7 signaling and CD127 receptor regulation in the control of T cell homeostasis. *Semin. Immunol.* **24**, 209–217 (2012).
9. den Braber, I. et al. Maintenance of peripheral naive T cells is sustained by thymus output in mice but not humans. *Immunity* **36**, 288–297 (2012).
10. Qi, Q. et al. Diversity and clonal selection in the human T-cell repertoire. *Proc. Natl Acad. Sci. USA* **111**, 13139–13144 (2014).
11. Li, G. et al. Decline in miR-181a expression with age impairs T cell receptor sensitivity by increasing DUSP6 activity. *Nat. Med.* **18**, 1518–1524 (2012).
12. Araujo, L., Khim, P., Mkhikian, H., Mortales, C. L. & Demetriou, M. Glycolysis and glutaminolysis cooperatively control T cell function by limiting metabolite supply to N-glycosylation. *eLife* **6**, e21330 (2017).
13. Chen, I. J., Chen, H. L. & Demetriou, M. Lateral compartmentalization of T cell receptor versus CD45 by galectin-N-glycan binding and microfilaments coordinate basal and activation signaling. *J. Biol. Chem.* **282**, 35361–35372 (2007).
14. Demetriou, M., Granovsky, M., Quaggin, S. & Dennis, J. W. Negative regulation of T-cell activation and autoimmunity by Mgat5 N-glycosylation. *Nature* **409**, 733–739 (2001).
15. Dennis, J. W., Nabi, I. R. & Demetriou, M. Metabolism, cell surface organization, and disease. *Cell* **139**, 1229–1241 (2009).
16. Lau, K. S. et al. Complex N-glycan number and degree of branching cooperate to regulate cell proliferation and differentiation. *Cell* **129**, 123–134 (2007).
17. Mkhikian, H. et al. Genetics and the environment converge to dysregulate N-glycosylation in multiple sclerosis. *Nat. Commun.* **2**, 334 (2011).
18. Mkhikian, H. et al. Golgi self-correction generates bioequivalent glycans to preserve cellular homeostasis. *eLife* **5**, e14814 (2016).
19. Mortales, C. L., Lee, S. U. & Demetriou, M. N-Glycan branching is required for development of mature B cells. *J. Immunol.* **205**, 630–636 (2020).
20. Morgan, R. et al. N-acetylglucosaminyltransferase V (Mgat5)-mediated N-glycosylation negatively regulates Th1 cytokine production by T cells. *J. Immunol.* **173**, 7200–7208 (2004).
21. Mortales, C. L., Lee, S. U., Manousadjian, A., Hayama, K. L. & Demetriou, M. N-Glycan branching decouples B Cell innate and adaptive immunity to control inflammatory demyelination. *iScience* **23**, 101380 (2020).
22. Dennis, J. W., Warren, C. E., Granovsky, M. & Demetriou, M. Genetic defects in N-glycosylation and cellular diversity in mammals. *Curr. Opin. Struct. Biol.* **11**, 601–607 (2001).

23. Sy, M. et al. N-Acetylglucosamine drives myelination by triggering oligodendrocyte precursor cell differentiation. *J. Biol. Chem.* **295**, 17413–17424 (2020).
24. Grigorian, A. & Demetriou, M. Mgat5 deficiency in T cells and experimental autoimmune encephalomyelitis. *ISRN Neurol.* **2011**, 374314 (2011).
25. Bahaie, N. S. et al. N-Glycans differentially regulate eosinophil and neutrophil recruitment during allergic airway inflammation. *J. Biol. Chem.* **286**, 38231–38241 (2011).
26. Li, C. F. et al. Hypomorphic MGAT5 polymorphisms promote multiple sclerosis cooperatively with MGAT1 and interleukin-2 and 7 receptor variants. *J. Neuroimmunol.* **256**, 71–76 (2013).
27. Zhou, R. W. et al. N-glycosylation bidirectionally extends the boundaries of thymocyte positive selection by decoupling Lck from Ca(2)(+) signaling. *Nat. Immunol.* **15**, 1038–1045 (2014).
28. Lee, S. U. et al. Increasing cell permeability of N-acetylglucosamine via 6-acetylation enhances capacity to suppress T-helper 1 (TH1)/TH17 responses and autoimmunity. *PLoS One* **14**, e0214253 (2019).
29. Grigorian, A. et al. Control of T Cell-mediated autoimmunity by metabolite flux to N-glycan biosynthesis. *J. Biol. Chem.* **282**, 20027–20035 (2007).
30. Lee, S. U. et al. N-glycan processing deficiency promotes spontaneous inflammatory demyelination and neurodegeneration. *J. Biol. Chem.* **282**, 33725–33734 (2007).
31. Park, J. H. et al. Suppression of IL7Ralpha transcription by IL-7 and other prosurvival cytokines: a novel mechanism for maximizing IL-7-dependent T cell survival. *Immunity* **21**, 289–302 (2004).
32. Becklund, B. R. et al. The aged lymphoid tissue environment fails to support naive T cell homeostasis. *Sci. Rep.* **6**, 30842 (2016).
33. Martin, C. E. et al. IL-7/anti-IL-7 mAb complexes augment cytokine potency in mice through association with IgG-Fc and by competition with IL-7R. *Blood* **121**, 4484–4492 (2013).
34. Grabstein, K. H. et al. Inhibition of murine B and T lymphopoiesis in vivo by an anti-interleukin 7 monoclonal antibody. *J. Exp. Med.* **178**, 257–264 (1993).
35. Martin, C. E. et al. Interleukin-7 availability is maintained by a hematopoietic cytokine sink comprising innate lymphoid cells and T cells. *Immunity* **47**, 171–182 e174 (2017).
36. Weitzmann, M. N., Roggia, C., Toraldo, G., Weitzmann, L. & Pacifici, R. Increased production of IL-7 uncouples bone formation from bone resorption during estrogen deficiency. *J. Clin. Invest.* **110**, 1643–1650 (2002).
37. Grigorian, A. et al. N-acetylglucosamine inhibits T-helper 1 (Th1)/T-helper 17 (Th17) responses and treats experimental autoimmune encephalomyelitis. *J. Biol. Chem.* **286**, 40133–40141 (2011).
38. Blaschitz, C. & Raffatellu, M. Th17 cytokines and the gut mucosal barrier. *J. Clin. Immunol.* **30**, 196–203 (2010).
39. Liu, J. Z., Pezeshki, M. & Raffatellu, M. Th17 cytokines and host-pathogen interactions at the mucosa: dichotomies of help and harm. *Cytokine* **48**, 156–160 (2009).
40. Parry, C. M. et al. A retrospective study of secondary bacteraemia in hospitalised adults with community acquired non-typhoidal *Salmonella gastroenteritis*. *BMC Infect. Dis.* **13**, 107 (2013).
41. Ren, Z. et al. Effect of age on susceptibility to *Salmonella* Typhimurium infection in C57BL/6 mice. *J. Med. Microbiol.* **58**, 1559–1567 (2009).
42. Raffatellu, M. et al. Simian immunodeficiency virus-induced mucosal interleukin-17 deficiency promotes *Salmonella* dissemination from the gut. *Nat. Med.* **14**, 421–428 (2008).
43. Geddes, K. et al. Identification of an innate T helper type 17 response to intestinal bacterial pathogens. *Nat. Med.* **17**, 837–844 (2011).
44. Vranjkovic, A., Crawley, A. M., Gee, K., Kumar, A. & Angel, J. B. IL-7 decreases IL-7 receptor alpha (CD127) expression and induces the shedding of CD127 by human CD8+ T cells. *Int. Immunol.* **19**, 1329–1339 (2007).
45. Sportes, C. et al. Administration of rhIL-7 in humans increases in vivo TCR repertoire diversity by preferential expansion of naive T cell subsets. *J. Exp. Med.* **205**, 1701–1714 (2008).
46. Kim, H. R., Hong, M. S., Dan, J. M. & Kang, I. Altered IL-7Rα expression with aging and the potential implications of IL-7 therapy on CD8+ T-cell immune responses. *Blood* **107**, 2855–2862 (2006).
47. Ucar, D. et al. The chromatin accessibility signature of human immune aging stems from CD8(+) T cells. *J. Exp. Med.* **214**, 3123–3144 (2017).
48. Abdel Rahman, A. M., Ryczko, M., Pawling, J. & Dennis, J. W. Probing the hexosamine biosynthetic pathway in human tumor cells by multitargeted tandem mass spectrometry. *ACS Chem. Biol.* **8**, 2053–2062 (2013).
49. Brandt, A. U. et al. Association of a marker of N-acetylglucosamine with progressive multiple sclerosis and neurodegeneration. *JAMA Neurol.* **78**, 842–852 (2021).
50. Passtoors, W. M. et al. IL7R gene expression network associates with human healthy ageing. *Immun. Ageing* **12**, 21 (2015).
51. Davey, D. A. Androgens in women before and after the menopause and post bilateral oophorectomy: clinical effects and indications for testosterone therapy. *Womens Health (Lond.)* **8**, 437–446 (2012).
52. Taylor, J. et al. Transcriptomic profiles of aging in naive and memory CD4(+) cells from mice. *Immun. Ageing* **14**, 15 (2017).
53. Gubbels Bupp, M. R., Potluri, T., Fink, A. L. & Klein, S. L. The confluence of sex hormones and aging on immunity. *Front. Immunol.* **9**, 1269 (2018).
54. Peckham, H. et al. Male sex identified by global COVID-19 meta-analysis as a risk factor for death and ITU admission. *Nat. Commun.* **11**, 6317 (2020).
55. Takahashi, T. et al. Sex differences in immune responses that underlie COVID-19 disease outcomes. *Nature* **588**, 315–320 (2020).
56. Bove, R. M. et al. Effect of gender on late-onset multiple sclerosis. *Mult. Scler.* **18**, 1472–1479 (2012).
57. Klein, S. L. & Flanagan, K. L. Sex differences in immune responses. *Nat. Rev. Immunol.* **16**, 626–638 (2016).
58. Fink, A. L. & Klein, S. L. Sex and gender impact immune responses to vaccines among the elderly. *Physiology (Bethesda)* **30**, 408–416 (2015).
59. Goss, P. E., Reid, C. L., Bailey, D. & Dennis, J. W. Phase IB clinical trial of the oligosaccharide processing inhibitor swainsonine in patients with advanced malignancies. *Clin. Cancer Res.* **3**, 1077–1086 (1997).
60. Grigorian, A. & Demetriou, M. Manipulating cell surface glycoproteins by targeting N-glycan-galectin interactions. *Methods Enzymol.* **480**, 245–266 (2010).

Acknowledgements

We thank C. Kawas (UC Irvine) for access to subjects from the '90+ cohort'. Research was supported by the National Institute of Allergy and Infectious Disease (R01AI108917, M.D.; R01AI144403, M.D.; R01AI126277, M.R.; R01AI114625, M.R.), the National Center for Complementary and Integrative Health (R01AT007452, M.D.), the Burroughs Wellcome Fund (Investigator in the Pathogenesis of Infectious Disease Award, M.R.) and a predoctoral fellowship from the American Heart Association (S.K.). The funders had no role in the study design, data collection and analysis, decision to publish or preparation of the manuscript. Obtaining human blood was supported by a Clinical Translational Science Award to the Institute for Clinical and Translation Science, UC Irvine.

Author contributions

H.M. and M.D. conceptualized the study. K.L.H., H.M., S.K., M.R., J.P., J.W.D. and M.D. developed the methodology. K.L.H., H.M., K.K., C.L., R.W.Z., J.P., S.K., P.Q.N.T, K.M.L., A.D.G., J.L.H., D.G., P.L.L., H.S. and B.L.N. performed the investigation. K.L.H, H.M. and M.D. wrote the original draft. H.M. and M.D. reviewed and edited the manuscript. K.L.H, H.M. and M.D. provided visualizations. H.M., M.R., J.W.D. and M.D. supervised the project. M.R. and M.D. acquired funding.

Competing interests

J.D. and M.D. are named as inventors on a patent application that describes GlcNAc as a biomarker for multiple sclerosis. J.D. and M.D. are named as inventors on a patent for use of GlcNAc in multiple sclerosis. The remaining authors declare no competing interests.

Additional information

Extended data is available for this paper at https://doi.org/10.1038/s43587-022-00187-y.

Supplementary information The online version contains supplementary material available at https://doi.org/10.1038/s43587-022-00187-y.

Correspondence and requests for materials should be addressed to Michael Demetriou.

Peer review information *Nature Aging* thanks Jung-Hyun Park and the other, anonymous, reviewer(s) for their contribution to the peer review of this work.

Reprints and permissions information is available at www.nature.com/reprints.

Publisher's note Springer Nature remains neutral with regard to jurisdictional claims in published maps and institutional affiliations.

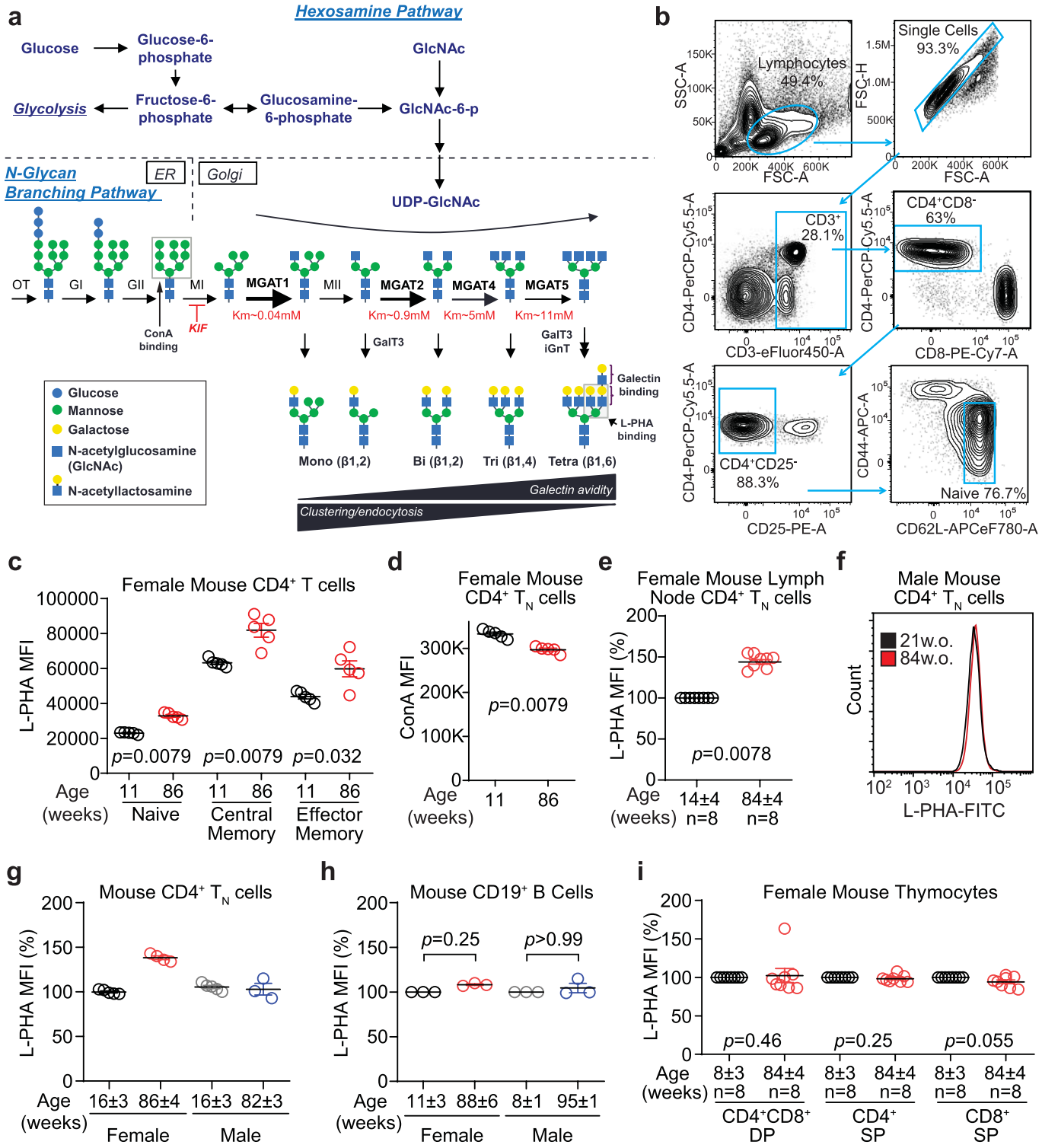

Extended Data Fig. 1 | See next page for caption.

Extended Data Fig. 1 | Mouse T cells display a sex-dimorphic increase in N-glycan branching with age. a) Fructose 6-phosphate may be metabolized by glycolysis or enter the hexosamine pathway to supply UDP-GlcNAc to the Golgi branching enzymes Mgat1, 2, 4 and 5, which generate mono-, bi-, tri-, and tetra-antennary GlcNAc branched glycans, respectively. The branching enzymes utilize UDP-GlcNAc with declining efficiency such that both Mgat4 and Mgat5 are limited for branching by the metabolic production of UDP-GlcNAc. Small molecule inhibitor kifunensine (KIF) can be used to eliminate N-glycan branching. Plant lectin L-PHA (*Phaseolus vulgaris*, leukoagglutinin) and ConA (concanavalin A) binding sites are also shown. Abbreviations: OT, oligosaccharyltransferases; GI, glucosidase I; GII, glucosidase II; MI, mannosidase I; MII, mannosidase II; Mgat, N-acetylglucosaminyltransferase; GalT3, galactosyltransferase 3; iGnT, i-branching enzyme β1,3-N-acetylglucosaminyltransferase; KIF, kifunensine; GlcNAc, N-acetylglucosamine; UDP, uridine diphosphate; Km, Michaelis constant of the enzyme. **b)** The gating strategy is demonstrated for $CD4^+$ T_N cells. Lymphocytes were first gated on singlets, followed by gating on $CD3^+CD4^+CD8^-CD25^-CD62L^+CD44^-$ cells by sequential steps. **c, d)** Splenocytes from five young and old mice were analyzed for L-PHA (**c**) or ConA (**d**) binding by flow cytometry, gating on the indicated $CD4^+$ T cell subsets. Absolute geometric mean fluorescence intensity (MFI) is shown to allow direct comparison between naive and memory subsets. **e-i)** $CD4^+$ T_N cells (**e-g**) $CD19^+$ B cells (**h**) or thymocytes (**i**) were obtained from the lymph node (**e**), spleen (**f-h**) or thymus (**i**) of female (**e, g-i**) or male (**f-h**) mice of the indicated ages, and analyzed for L-PHA binding by flow cytometry. Absolute or normalized geometric mean fluorescence intensity (MFI) are shown. Each symbol represents a single mouse. P-values by two-tailed Mann–Whitney (**c, d**) or two-tailed Wilcoxon (**e, h, i**). Error bars indicate mean ± s.e.m.

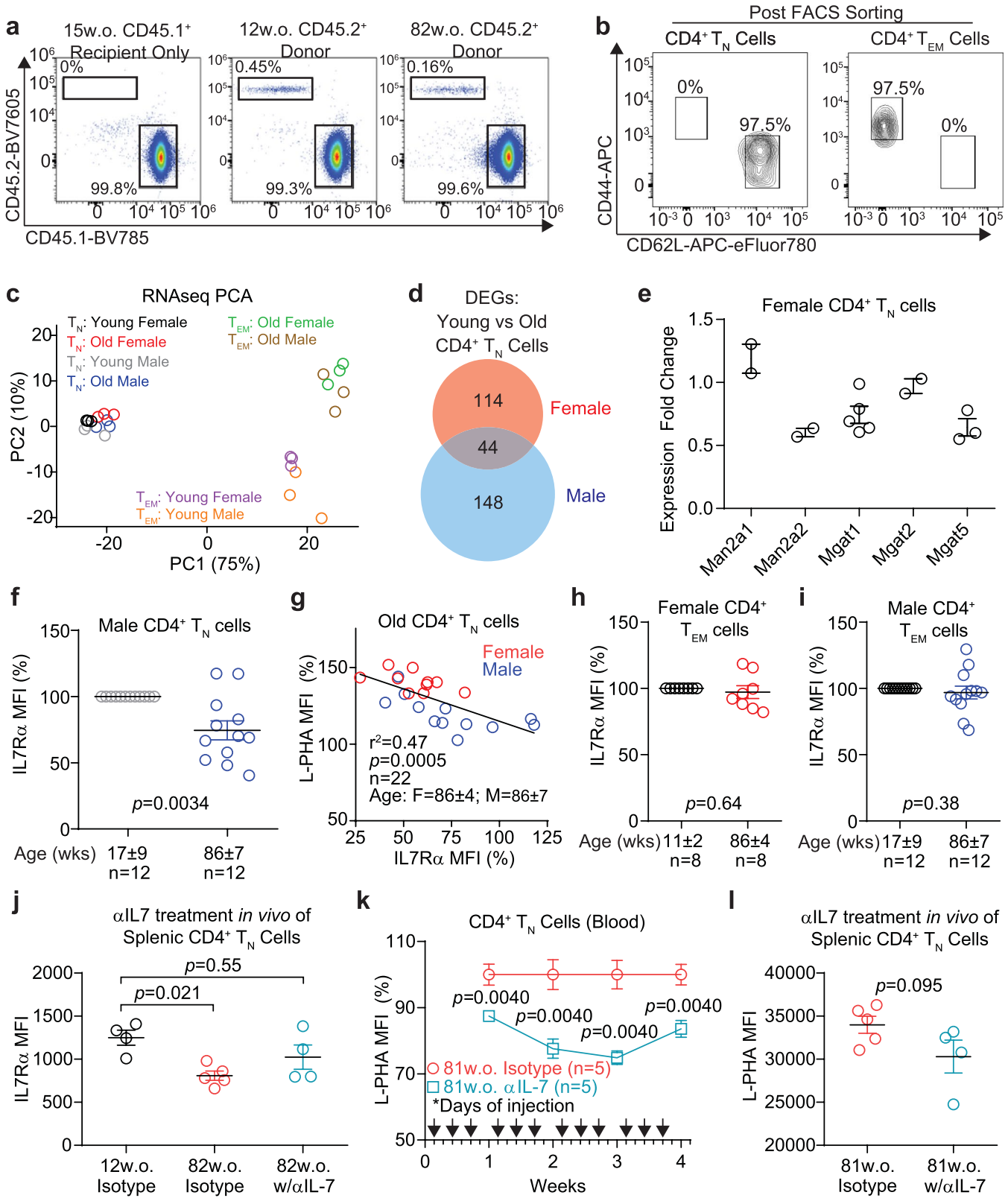

Extended Data Fig. 2 | See next page for caption.

Extended Data Fig. 2 | Elevated IL-7 signaling increases N-glycan branching in old female naiveT cells. a) Representative flow cytometry plots of donor and recipient cells post-adoptive transfer. **b)** Negatively selected CD4$^+$ T cells were FACS sorted for T_N (CD62L$^+$CD44$^-$) and T_{EM} (CD62L$^-$CD44$^+$) populations. Representative flow cytometry plots demonstrating purity of sorted cells used for RNA-seq. **c)** Principal component analysis (PCA) of RNA-seq data comparing gene expression in CD4$^+$ T_N and CD4$^+$ T_{EM} cells from young male (7-8 weeks old), young female (10-11 weeks old), old male (83-86 weeks old) and old female (85 weeks old) mice. Three biological replicates were performed for each group. **d)** Out of 24062 genes analyzed by RNA-seq, 158 DEGs were identified when comparing young and old CD4$^+$ T_N cells in females, 192 DEGs were identified in males, and 44 DEGs were shared. **e)** Young and old naive CD4$^+$ T cell mRNA expression of N-glycan pathway genes by real-time qPCR. **f)** Flow cytometric analysis of IL7Rα in *ex vivo* CD4$^+$ T_N cells from young and old male mice. **g)** L-PHA versus IL7Rα expression in *ex vivo* CD4$^+$ T_N cells from old male and female mice. **h, i)** Flow cytometric analysis of IL7Rα in *ex vivo* young and old CD4$^+$ T_{EM} cells from female (**h**) and male (**i**) mice. **j-l)** C57BL/6 mice of the indicated ages were injected intraperitoneally with either isotype control (1.5 mg) or anti-IL-7 antibody (M25, 1.5 mg) three times per week for two (**j**) or four (**k, l**) weeks, and analyzed for L-PHA or IL7Rα expression in blood (**k**) or spleen (**j, l**). Each symbol represents a single mouse unless specified otherwise. P-values determined by one-tailed Wilcoxon (**f**), linear regression (**g**), two-tailed Wilcoxon (**h, i**), Kruskal–Wallis with Dunn's multiple comparisons test (**j**), or one-tailed Mann–Whitney (**k, l**). Error bars indicate mean ± s.e.m.

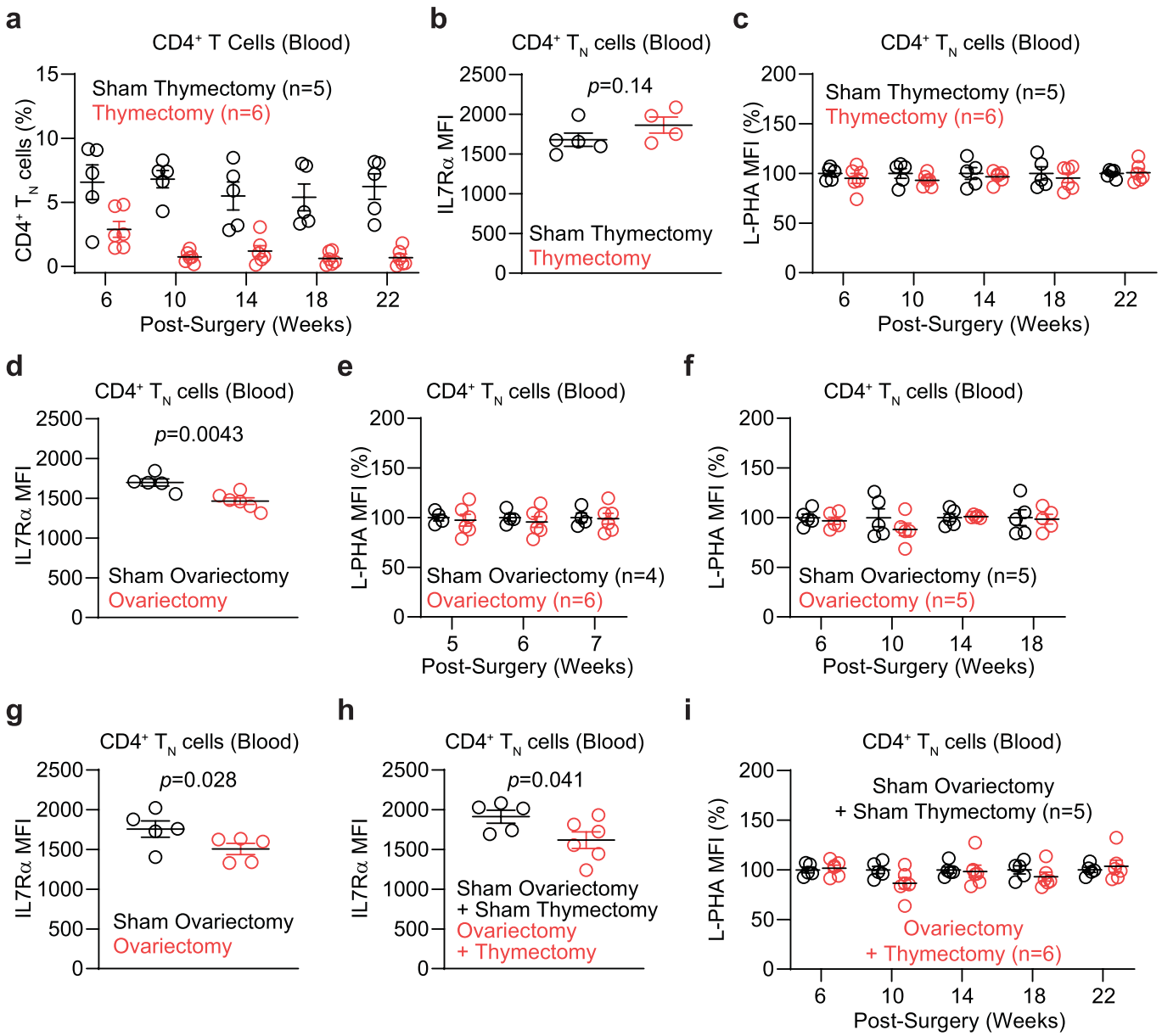

Extended Data Fig. 3 | Thymectomy and ovariectomy are insufficient to drive increases in N-glycan branching. a-i) Female mice underwent thymectomy (**a-c**), ovariectomy (**d-g**), both surgeries (**h, i**), or corresponding sham procedures at the age of 9 weeks. Flow cytometry on blood at the indicated timepoints post-procedure was performed to detect percentage of CD4$^+$ T_N cells (**a**), IL7Rα expression (**b, d, g, h**), or L-PHA binding (**c, e, f, i**), gating on CD4$^+$ T_N cells. Absolute or normalized geometric mean fluorescence intensity (MFI) are shown. Each symbol at a particular timepoint represents a single mouse. P-values determined by one-tailed Mann–Whitney (**b, d, g, h**). Error bars indicate mean ± s.e.m.

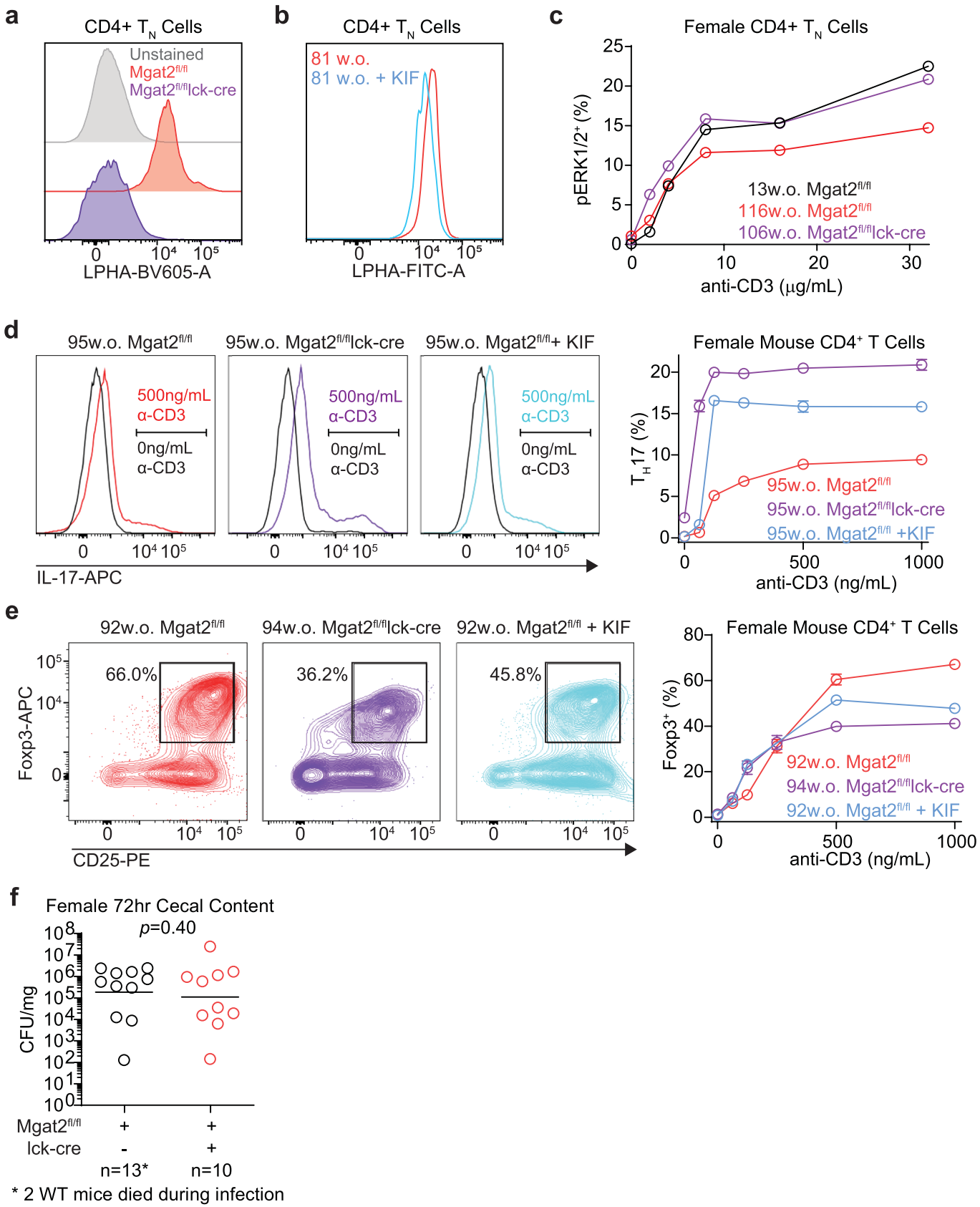

Extended Data Fig. 4 | See next page for caption.

Extended Data Fig. 4 | Age-dependent increases in N-glycan branching suppress proinflammatory T cell function. a) L-PHA binding of splenocytes from *Mgat2*$^{fl/fl}$ and *Mgat2*$^{fl/fl}$*lck-cre* female mice, gated on CD4$^+$ T_N cells. **b)** Splenocytes from an old mouse were treated with or without kifunensine for 24 hours, then analyzed for L-PHA binding by flow cytometry, gating on CD4$^+$ T_N cells. **c)** Splenocytes from female mice of the indicated ages and genotypes were activated with plate-bound anti-CD3 for 15 minutes. Following fixation and permeabilization, phospho-ERK1/2 induction was analyzed in CD4$^+$ T_N cells by flow cytometry, gating additionally on L-PHA negative cells in *Mgat2*$^{fl/fl}$*/lck-cre* mice. **d, e)** Flow cytometric analysis of purified mouse splenic CD4$^+$ T cells activated with anti-CD3 and anti-CD28 for 4 days with T_H17 (TGFβ + IL-6+IL-23) or iTreg (TGFβ) inducing conditions, gating additionally on L-PHA negative cells in *Mgat2*$^{fl/fl}$*/lck-cre* mice. **f)** Female *Mgat2*$^{fl/fl}$ and *Mgat2*$^{fl/fl}$*lck-cre* mice were inoculated with streptomycin (0.1 ml of a 200 mg/ml solution in sterile water) intragastrically one day prior to inoculation with *S.* Typhimurium (5×10^8 colony forming units, CFU per mouse) by oral gavage. CFU in the cecal content was determined 72 hours after infection. Data shown are representative of two (**c**), or at least three (**a, b, d, e**) independent experiments. P-values by one-tailed Mann–Whitney (**f**). Error bars indicate mean ± s.e.m (**c, d, e**) or geometric mean (**f**).

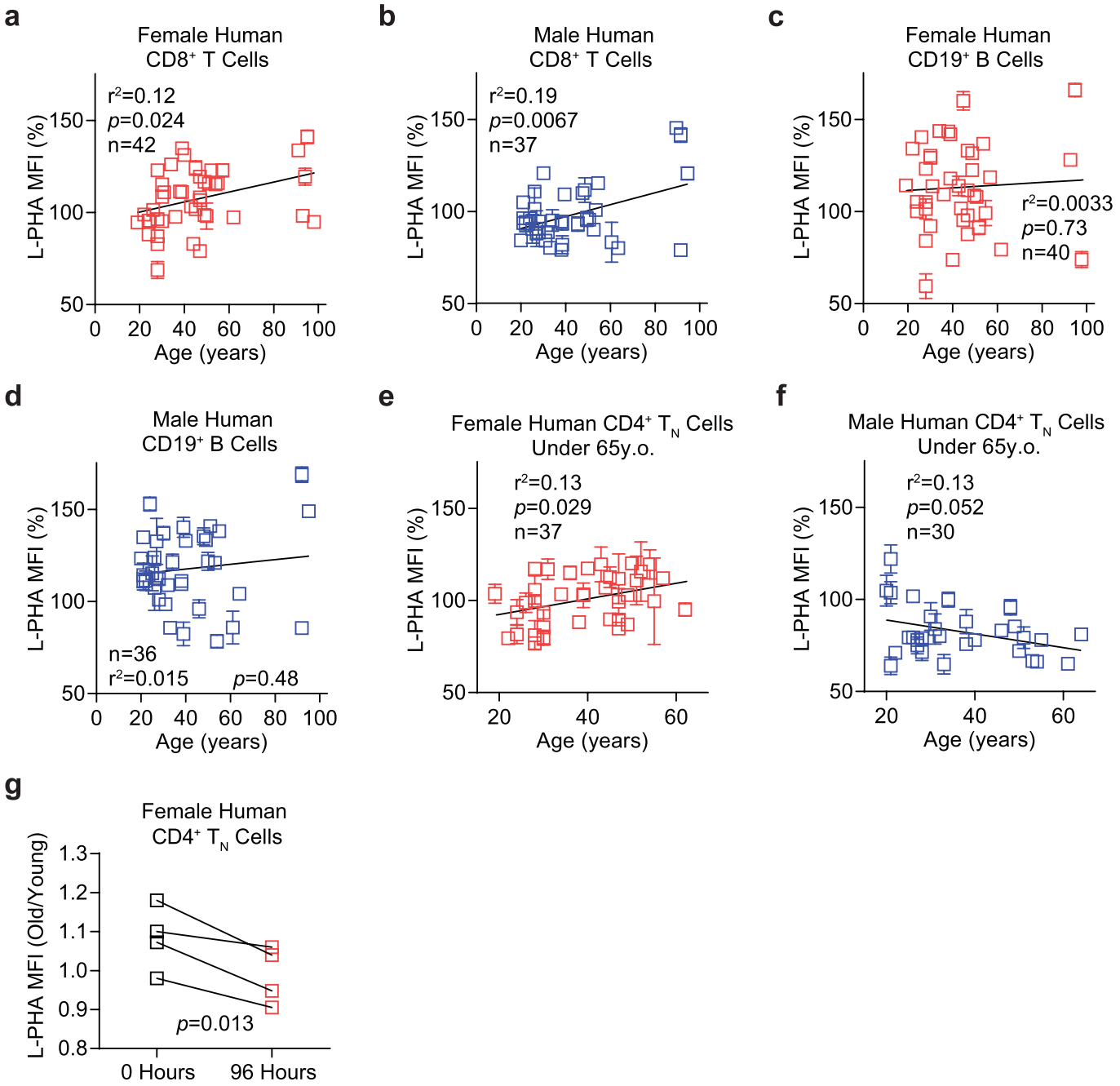

Extended Data Fig. 5 | Age-dependent increases in N-glycan branching suppress T cell activity in human females. a-d) Human PBMCs from healthy females (**a, c**) or males (**b, d**) as indicated were analyzed for L-PHA binding by flow cytometry gating on CD8$^+$ T cells (**a, b**) or CD19$^+$ B cells (**c, d**). **e, f)** CD4$^+$ T_N cells (CD45RA$^+$CD45RO$^-$) from healthy females (**e**) and males (**f**) under the age of 65 were analyzed for L-PHA binding by flow cytometry. **g)** Human PBMCs from young (22-38 years old) and old (90-94 years old) female subjects were analyzed for L-PHA binding on CD4$^+$ T_N cells (CD45RA$^+$CD45RO$^-$) before or after 96 hours of culture in complete media. Shown is the ratio or each old subject over the average of the young at the two timepoints. Each symbol represents a single individual. R^2 and p-values by linear regression (**a-f**) or by paired one-tailed t test, following passage of Shapiro–Wilk normality test (**g**). Error bars indicate mean ± s.e.m.

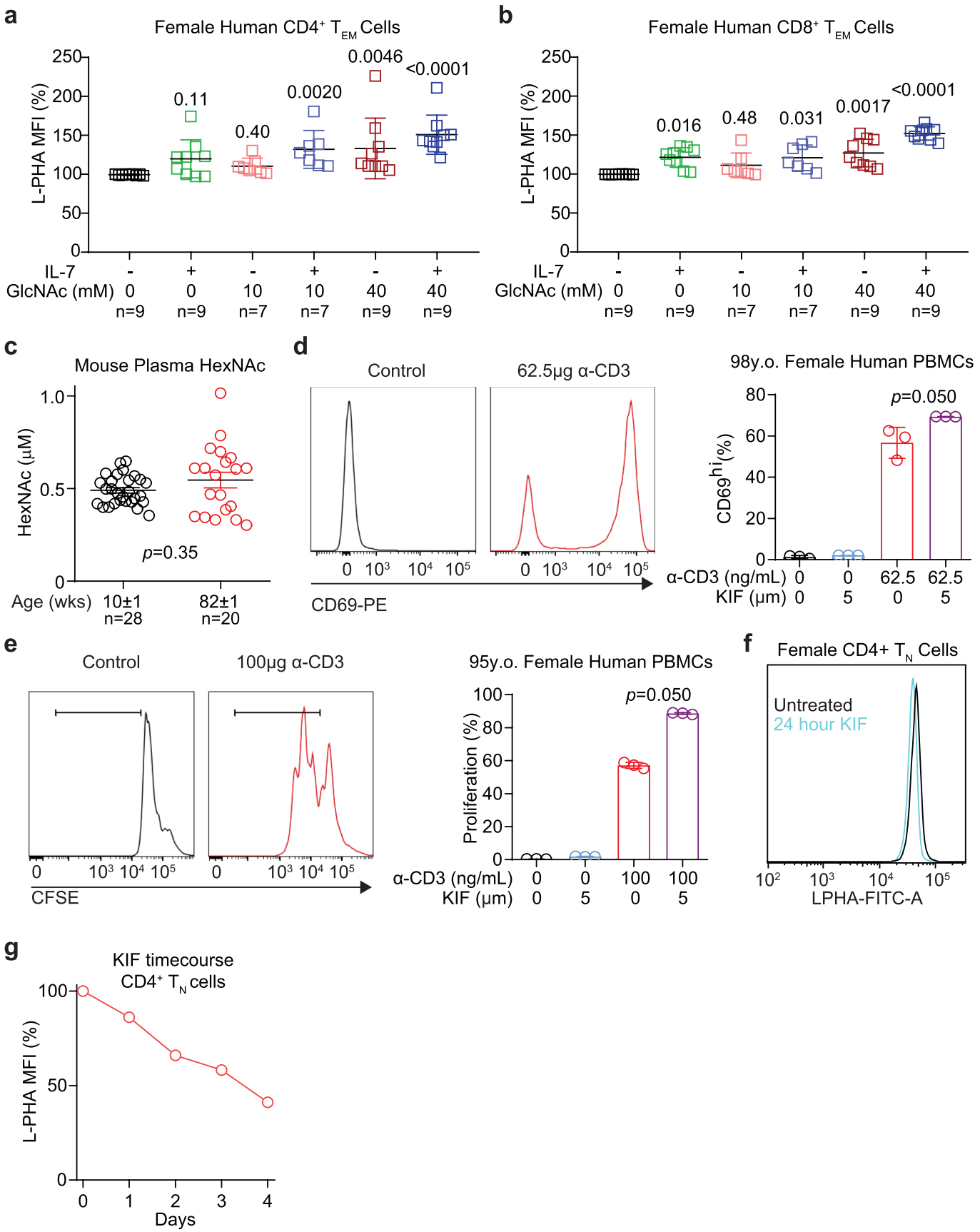

Extended Data Fig. 6 | See next page for caption.

Extended Data Fig. 6 | N-acetylglucosamine and IL-7 synergize to raise N-glycan branching in human T cells. a, b) PBMCs from nine healthy female donors (28-45 years old) were cultured with or without rhIL-7 (50 ng/ml) and/or GlcNAc (10 mM or 40 mM) for 9 days, then analyzed for L-PHA binding by flow cytometry, gating on $CD4^+$ T_{EM} ($CD45RA^-CD45RO^+CCR7^-$) cells (**a**) or $CD8^+$ T_{EM} ($CD45RA^-CD45RO^+CCR7^-$) cells (**b**). **c)** Mouse plasma from female mice of the indicated ages was analyzed for HexNAc levels by LC-MS/MS. **d, e)** Flow cytometric analysis of human PBMCs stimulated by anti-CD3 in the presence or absence of kifunensine as indicated for 24 hours to analyze for activation marker CD69 (**d**) or 72 hours to assess proliferation by CFSE dilution (**e**), gating on $CD4^+$ T cells. **f**) Female human PBMCs were treated in vitro with kifunensine for 24 hours, followed by analysis of L-PHA binding on $CD4^+$ T_N cells by flow cytometry. Data shown is representative of three independent experiments with different donors. **g**) Female human PBMCs were treated *in vitro* with kifunensine for up to four days, followed by analysis of L-PHA binding on $CD4^+$ T_N cells by flow cytometry. P-values by Kruskal–Wallis with Dunn's multiple comparisons test (**a, b**), two-tailed Mann–Whitney (**c**), and one-tailed Mann–Whitney (**d, e**). Error bars indicate mean ± s.e.m.

nature portfolio

Corresponding author(s): Michael Demetriou

Last updated by author(s): Jan 23, 2022

Reporting Summary

Nature Portfolio wishes to improve the reproducibility of the work that we publish. This form provides structure for consistency and transparency in reporting. For further information on Nature Portfolio policies, see our Editorial Policies and the Editorial Policy Checklist.

Statistics

For all statistical analyses, confirm that the following items are present in the figure legend, table legend, main text, or Methods section.

n/a	Confirmed
☐	☒ The exact sample size (*n*) for each experimental group/condition, given as a discrete number and unit of measurement
☐	☒ A statement on whether measurements were taken from distinct samples or whether the same sample was measured repeatedly
☐	☒ The statistical test(s) used AND whether they are one- or two-sided *Only common tests should be described solely by name; describe more complex techniques in the Methods section.*
☒	☐ A description of all covariates tested
☐	☒ A description of any assumptions or corrections, such as tests of normality and adjustment for multiple comparisons
☐	☒ A full description of the statistical parameters including central tendency (e.g. means) or other basic estimates (e.g. regression coefficient) AND variation (e.g. standard deviation) or associated estimates of uncertainty (e.g. confidence intervals)
☐	☒ For null hypothesis testing, the test statistic (e.g. *F*, *t*, *r*) with confidence intervals, effect sizes, degrees of freedom and *P* value noted *Give P values as exact values whenever suitable.*
☒	☐ For Bayesian analysis, information on the choice of priors and Markov chain Monte Carlo settings
☒	☐ For hierarchical and complex designs, identification of the appropriate level for tests and full reporting of outcomes
☐	☒ Estimates of effect sizes (e.g. Cohen's *d*, Pearson's *r*), indicating how they were calculated

Our web collection on statistics for biologists contains articles on many of the points above.

Software and code

Policy information about availability of computer code

Data collection	No software was used.
Data analysis	Data was analysed in Graphpad Prism Version 8. Flow cytometry data was analyzed in FlowJo Version 10. For RNAseq, the quality of the sequencing was first assessed using fastQC tool (v0.11.2). Raw reads were then adapter and quality trimmed and filtered by a length of 20 bases using trimmomatic (v0.35). Trimmed reads were mapped to the mouse mm10 reference genome using a splice aware aligner Tophat2 (v2.1.0) and resulting BAM files were processed using samtools (v.1.3), and gene expression was quantified with featureCounts (subread v2.0.1, featureCounts v1.5.0-p3) as raw counts and cufflinks (v2.2.1) as FPKM values. Raw counts were normalized and differential analysis was done using R package DESeq2 (v1.22.2).

For manuscripts utilizing custom algorithms or software that are central to the research but not yet described in published literature, software must be made available to editors and reviewers. We strongly encourage code deposition in a community repository (e.g. GitHub). See the Nature Portfolio guidelines for submitting code & software for further information.

Data

Policy information about availability of data

All manuscripts must include a data availability statement. This statement should provide the following information, where applicable:

- Accession codes, unique identifiers, or web links for publicly available datasets
- A description of any restrictions on data availability
- For clinical datasets or third party data, please ensure that the statement adheres to our policy

RNA-seq data has been deposited with the Gene Expression Omnibus under accession number GSE184496. The mouse 10mm reference genome was obtained from

https://hgdownload.soe.ucsc.edu/downloads.html#mouse. Source data is provided for all main and extended data figures in supplemental information. Additional data that support the findings within this article are available from the corresponding author upon reasonable request.

Field-specific reporting

Please select the one below that is the best fit for your research. If you are not sure, read the appropriate sections before making your selection.

☒ Life sciences ☐ Behavioural & social sciences ☐ Ecological, evolutionary & environmental sciences

For a reference copy of the document with all sections, see nature.com/documents/nr-reporting-summary-flat.pdf

Life sciences study design

All studies must disclose on these points even when the disclosure is negative.

Sample size	No statistical methods were used to pre-determine sample sizes but sample sizes were based on our previous experience performing comparable experiments and were similar to those reported in previous publications (Ref 11, 18). For mouse analysis, an n of 3 or greater per group was used as indicated in figures and/or legends.
Data exclusions	For all flow cytometry data, non-viable cells and doublets were excluded. In flow cytometry experiments, individual replicates were excluded if fluidics errors such as bubbles or clogging were detected during sample collection and significantly altered scattering characteristics or event counts. In Figure 2h, one mouse in the "12w.o. Isotype" group died on day 8, likely due to mishandling/misinjection, and could not be included in the 2 week time point. In Fig. 4b, one data point in the Mgat2fl/fl group could not be included due to failed MLN dissection. Data from experiments where positive and/or negative controls failed were excluded.
Replication	All attempts at replication were successful. For ex vivo measurements each data point is a single mouse or human, and therefore each data point is an independent replicate. For in vitro experiments data are representative of multiple independent experiments as defined in the figure legends. RNAseq was performed once, using cells purified from pairs of young and old mice on three separate days. For adoptive transfer (Fig. 2b) and in vivo salmonella experiments (Fig. 4), each data point is an independent replicate.
Randomization	Mice and humans were randomly selected and assessed. Mouse littermates were randomly distributed into treatment groups for in vivo experiments. Human participants were randomly enrolled and allocated based on age and gender.
Blinding	As physical attributes of mice are the same, no blinding was performed for mouse experiments. Human subjects were not blinded as this was an observational study rather than a clinical trial. The individuals performing serum measurements were blinded to sex and age. Quantification by flow cytometry was performed in a uniform manner for all samples.

Reporting for specific materials, systems and methods

We require information from authors about some types of materials, experimental systems and methods used in many studies. Here, indicate whether each material, system or method listed is relevant to your study. If you are not sure if a list item applies to your research, read the appropriate section before selecting a response.

Materials & experimental systems

n/a	Involved in the study
☐	☒ Antibodies
☒	☐ Eukaryotic cell lines
☒	☐ Palaeontology and archaeology
☐	☒ Animals and other organisms
☐	☒ Human research participants
☒	☐ Clinical data
☒	☐ Dual use research of concern

Methods

n/a	Involved in the study
☒	☐ ChIP-seq
☐	☒ Flow cytometry
☒	☐ MRI-based neuroimaging

Antibodies

Antibodies used

Anti-mouse flow cytometry antibodies:
Anti-CD69-PE (H1.2F3); ThermoFisher Scientific Cat#12-0691-82
Anti-IL17-APC (eBio17B7); ThermoFisher Scientific Cat#17-7177-81
Anti-CD4-PerCP-Cy5.5 (RM4-5); ThermoFisher Scientific Cat#45-0042-82
Anti-CD8α-PE-Cy7 (53-6.7); ThermoFisher Scientific Cat#25-0081-82
Anti-CD19-APC (1D3); ThermoFisher Scientific Cat#17-0193-82
Anti-Foxp3-APC (Fjk-16s); ThermoFisher Scientific Cat#17-5773-82
Anti-CD44-APC (IM7); ThermoFisher Scientific Cat#17-0441-82
Anti-CD62L-APC-eFluor780 (MEL-14); ThermoFisher Scientific Cat#47-0621-82
Anti-CD3-eFluor450 (145-2C11); ThermoFisher Scientific Cat#48-0031-82
Anti-CD25-PE (PC61.5); ThermoFisher Scientific Cat#12-0251-82

Anti-IL7Rα-PE (A7R34); ThermoFisher Scientific Cat#12-1271-82
Anti-Phospho-STAT5-FITC (SRBCZX); ThermoFisher Scientific Cat#11-9010-42
Anti-Phospho-CD247-PE (3ZBR4S); ThermoFisher Scientific Cat# 12-2478-42
Anti-Phospho-Zap70-PE (n3kobu5); ThermoFisher Scientific Cat# 12-9006-42
Anti-CD45.1-BV785 (A20); BioLegend Cat#110743
Anti-CD45.2-BV605 (104); BioLegend Cat#109841
Anti-Phospho-ERK1/2-Alexa Fluor 488 (4B11B69); BioLegend Cat#675508

Anti-human flow cytometry antibodies:
Anti-Phospho-ERK1/2-PE (MILAN8R); ThermoFisher Scientific Cat#17-9109-42
Anti-CD45RA-PE-Cy7 (HI100); ThermoFisher Scientific Cat#25-0458-42
Anti-CD4-PerCP-Cy5.5 (RM4-5); ThermoFisher Scientific Cat#45-0042-82
Anti-CCR7-PE (4B12); ThermoFisher Scientific Cat#12-1971-82
Anti-CD25-PerCP-Cy5.5 (BC96); ThermoFisher Scientific Cat#45-0259-42
Anti-CD19-APC (HIB19); ThermoFisher Scientific Cat#17-0199-42
Anti-CD45RO-APC (UCHL1); BioLegend Cat#304210
Anti-CD8-PE-Cy7 (SK1); BioLegend Cat#344750

In vivo antibodies:
Anti-IL7 (M25); BioXCell Cat#BE0048
Mouse IgG2bK isotype control (MPC-11); BioXCell Cat#BE0086

Lectins used for flow cytometry:
L-PHA-Fluorescein; Vector Labs Cat#FL-1111-2
L-PHA-biotinylated; Vector Labs Cat#B-1115-2
Conconavalin A-Fluorescein; Vector Labs Cat#FL-1001-25

Validation

All antibodies used are validated by the manufacturer and validation descriptions provided on their websites. Using the above catalog numbers, validation information is available at www.biolegend.com or www.thermofisher.com. Furthermore, the antibodies and clones used are well established in the immunology field and used routinely by us with reproducible results. L-PHA binding by flow cytometry has been validated as a sensitive, specific, and quantitative measure of N-glycan branching by us and others previously (Ref 17, 18, 29). The functional anti-IL7 M25 antibody has been previously validated (Ref 33, 34).

Validation information for the flow cytometry antibodies used can be found in the datasheets linked below:

Anti-CD69-PE (H1.2F3); https://www.thermofisher.com/order/genome-database/dataSheetPdf?producttype=antibody&productsubtype=antibody_primary&productId=12-0691-82&version=202

Anti-IL17-APC (eBio17B7); https://www.thermofisher.com/order/genome-database/dataSheetPdf?producttype=antibody&productsubtype=antibody_primary&productId=17-7177-81&version=202

Anti-CD4-PerCP-Cy5.5 (RM4-5); https://www.thermofisher.com/order/genome-database/dataSheetPdf?producttype=antibody&productsubtype=antibody_primary&productId=45-0042-82&version=202

Anti-CD8α-PE-Cy7 (53-6.7); https://www.thermofisher.com/order/genome-database/dataSheetPdf?producttype=antibody&productsubtype=antibody_primary&productId=25-0081-82&version=202

Anti-CD19-APC (1D3); https://www.thermofisher.com/order/genome-database/dataSheetPdf?producttype=antibody&productsubtype=antibody_primary&productId=17-0193-82&version=202

Anti-Foxp3-APC (Fjk-16s); https://www.thermofisher.com/order/genome-database/dataSheetPdf?producttype=antibody&productsubtype=antibody_primary&productId=17-5773-82&version=202

Anti-CD44-APC (IM7); https://www.thermofisher.com/order/genome-database/dataSheetPdf?producttype=antibody&productsubtype=antibody_primary&productId=17-0441-82&version=202

Anti-CD62L-APC-eFluor780 (MEL-14); https://www.thermofisher.com/order/genome-database/dataSheetPdf?producttype=antibody&productsubtype=antibody_primary&productId=47-0621-82&version=202

Anti-CD3-eFluor450 (145-2C11); https://www.thermofisher.com/order/genome-database/dataSheetPdf?producttype=antibody&productsubtype=antibody_primary&productId=48-0031-82&version=202

Anti-CD25-PE (PC61.5); https://www.thermofisher.com/order/genome-database/dataSheetPdf?producttype=antibody&productsubtype=antibody_primary&productId=12-0251-82&version=202

Anti-IL7Rα-PE (A7R34); https://www.thermofisher.com/order/genome-database/dataSheetPdf?producttype=antibody&productsubtype=antibody_primary&productId=12-1271-82&version=202

Anti-Phospho-STAT5-FITC (SRBCZX); https://www.thermofisher.com/order/genome-database/dataSheetPdf?producttype=antibody&productsubtype=antibody_primary&productId=11-9010-42&version=202

Anti-Phospho-CD247-PE (3ZBR4S); https://www.thermofisher.com/order/genome-database/dataSheetPdf?producttype=antibody&productsubtype=antibody_primary&productId=12-2478-42&version=202

Anti-Phospho-Zap70-PE (n3kobu5); https://www.thermofisher.com/order/genome-database/dataSheetPdf?producttype=antibody&productsubtype=antibody_primary&productId=12-9006-42&version=202

Anti-CD45.1-BV785 (A20); https://www.biolegend.com/en-us/global-elements/pdf-popup/brilliant-violet-785-anti-mouse-cd45-1-antibody-9654?filename=Brilliant%20Violet%20785trade%20anti-mouse%20CD451%20Antibody.pdf&pdfgen=true

Anti-CD45.2-BV605 (104); https://www.biolegend.com/en-us/global-elements/pdf-popup/brilliant-violet-605-anti-mouse-cd45-2-antibody-9695?filename=Brilliant%20Violet%20605trade%20anti-mouse%20CD452%20Antibody.pdf&pdfgen=true

Anti-Phospho-ERK1/2-Alexa Fluor 488 (4B11B69); https://www.biolegend.com/en-us/global-elements/pdf-popup/alexa-fluor-488-anti-erk1-2-phospho-thr202-tyr204-antibody-13656?filename=Alexa%20Fluorreg%20488%20anti-ERK12%20Phospho%20Thr202Tyr204%20Antibody.pdf&pdfgen=true

Anti-Phospho-ERK1/2-PE (MILAN8R); https://www.thermofisher.com/order/genome-database/dataSheetPdf?producttype=antibody&productsubtype=antibody_primary&productId=17-9109-42&version=202

Anti-CD45RA-PE-Cy7 (HI100); https://www.thermofisher.com/order/genome-database/dataSheetPdf?producttype=antibody&productsubtype=antibody_primary&productId=25-0458-42&version=202

Anti-CD4-PerCP-Cy5.5 (RM4-5); https://www.thermofisher.com/order/genome-database/dataSheetPdf?producttype=antibody&productsubtype=antibody_primary&productId=45-0042-82&version=202

Anti-CCR7-PE (4B12); https://www.thermofisher.com/order/genome-database/dataSheetPdf?producttype=antibody&productsubtype=antibody_primary&productId=12-1971-82&version=202

Anti-CD25-PerCP-Cy5.5 (BC96); https://www.thermofisher.com/order/genome-database/dataSheetPdf?producttype=antibody&productsubtype=antibody_primary&productId=45-0259-42&version=202

Anti-CD19-APC (HIB19); https://www.thermofisher.com/order/genome-database/dataSheetPdf?producttype=antibody&productsubtype=antibody_primary&productId=17-0199-42&version=202

Anti-CD45RO-APC (UCHL1); https://www.biolegend.com/en-us/global-elements/pdf-popup/apc-anti-human-cd45ro-antibody-856?filename=APC%20anti-human%20CD45RO%20Antibody.pdf&pdfgen=true

Anti-CD8-PE-Cy7 (SK1); https://www.biolegend.com/en-us/global-elements/pdf-popup/pe-cyanine7-anti-human-cd8-antibody-6390?filename=PECyanine7%20anti-human%20CD8%20Antibody.pdf&pdfgen=true

Animals and other organisms

Policy information about studies involving animals; ARRIVE guidelines recommended for reporting animal research

Laboratory animals	All mouse experiments utilized C57BL/6 mice. C57BL/6 Mgat2f/f and Mgat2f/fLck-Cre were bred in house by initially crossing Mgat2f/f (JAX #006892) and Lck-Cre (JAX #003802) mice and are previously described (Ref 27). Young and aged wild-type C57BL/6 mice were obtained from the National Institute of Aging (NIA) colony maintained at Charles River Laboratories (Wilmington, MA, USA). Cd45.1 (JAX #002014) C57BL/6 mice were obtained from JAX. C57BL/6 mice were ovariectomized, thymectomized, ovariectomized and thymectomized, or subject to sham surgery by JAX surgical services at 9 weeks of age. For all experiments, delivered animals were allowed to acclimate to our vivarium for at least one week prior to measurements or the start of experiments. Mice were housed at the University of California, Irvine in an environment-controlled, pathogen-free barrier facility on a 12-h/12-h light/dark cycle at a constant temperature and humidity, with food and water available ad libitum. Young mice were 7-32 weeks old, while old mice were 74-130 weeks old. Age and sex information for particular experiments is indicated in the figures and/or figure legends. The Institutional Animal Care and Use Committee of the University of California, Irvine, approved all mouse experiments and protocols (protocol number AUP-19-157).
Wild animals	The study did not involve wild animals.
Field-collected samples	The study did not involve field-collected samples.
Ethics oversight	The Institutional Animal Care and Use Committee of the University of California, Irvine, approved all mouse experiments and protocols (protocol number AUP-19-157).

Note that full information on the approval of the study protocol must also be provided in the manuscript.

Human research participants

Policy information about studies involving human research participants

Population characteristics	Male and females subjects with an age range of 19-98 years old were examined in this study. Age and sex for particular experiments are indicated in the figures and/or figure legends. Individuals with cancer, uncontrolled medical disease or any other inflammatory syndrome were excluded. Human whole blood was collected from healthy individuals through the Research Blood Donor Program serviced by the Institute for Clinical & Translational Science (ICTS) or through The 90+ Study at the University of California, Irvine. All procedures with human subjects were approved by the Institutional Review Board of the University of California, Irvine. All study participants gave written informed consent and were uncompensated.
Recruitment	Healthy individuals were recruited through the Research Blood Donor Program serviced by the Institute for Clinical & Translational Science (ICTS) or through the 90+ Study at the University of California, Irvine (UCI). As age and sex were the primary allocation, there was no self-selection for these parameters.

Ethics oversight	All procedures with human subjects were approved by the Institutional Review Board of the University of California, Irvine.

Note that full information on the approval of the study protocol must also be provided in the manuscript.

Flow Cytometry

Plots

Confirm that:

☒ The axis labels state the marker and fluorochrome used (e.g. CD4-FITC).

☒ The axis scales are clearly visible. Include numbers along axes only for bottom left plot of group (a 'group' is an analysis of identical markers).

☒ All plots are contour plots with outliers or pseudocolor plots.

☒ A numerical value for number of cells or percentage (with statistics) is provided.

Methodology

Sample preparation	Human PBMCs were isolated by density gradient centrifugation over Histopaque-1077 (Sigma-Aldrich) or Lymphoprep (StemCell Technologies). Mouse ex vivo thymic, splenic, peripheral blood, and lymph node cell suspensions were analyzed for L-PHA binding by flow cytometry after erythrocyte depletion. For RNAseq and adoptive transfer experiments, splenic and lymph node CD4+ T cells were isolated using EasySep CD4+ T cell isolation kits (StemCell technologies) followed by cell sorting on a BD FACSAria Fusion Sorter for either naïve (CD3+CD4+CD25-CD62L+CD44-) or memory (CD3+CD4+CD25-CD62L-CD44+) populations.
Instrument	Flow cytometry was performed using an Attune NxT (Thermo Fisher Scientific), BD LSR II, or Novocyte 3000 (ACEA). Cell sorting was performed with a BD FACSAria Fusion Sorter.
Software	Data analysis was performed with FlowJo version 10.
Cell population abundance	For flow cytometry analysis representative plots demonstrating cell abundance are noted in the figures. For cell sorting of naive and memory CD4+ T cells from young and old, male and female mice, cell purity was >95%.
Gating strategy	An example of our gating strategy is provided in Supplementary Figure 1b. Mouse splenocytes are first gated for lymphocytes by FSC-A/SSC-A followed by gating on singlets by FSC-A/FSC-H and SSC-H/Width. CD3+CD4+CD8-CD25- cells are then gated in successive steps. Finally naive (CD62L+CD44-), central memory (CD62L+CD44+) and effector memory (CD62L-CD44+) cells are gated based on CD62L and CD44 expression. Gating was based on established protocols, single stains, FMO controls, and/or clear boundaries between negative and positive populations.

☒ Tick this box to confirm that a figure exemplifying the gating strategy is provided in the Supplementary Information.